Ultracold erbium atoms in a quasi-electrostatic optical dipole trap

Roberto Vittorio Röll

Masterarbeit in Physik
angefertigt im Institut für Angewandte Physik

vorgelegt der
Mathematisch-Naturwissenschaftlichen Fakultät
der
Rheinischen Friedrich-Wilhelms-Universität
Bonn

Oktober 2016

I hereby declare that this thesis was formulated by myself and that no sources or tools other than those cited were used.

Bonn, ...

Date Signature

1. Gutachter: Prof. Dr. Martin Weitz

2. Gutachterin: Priv.-Doz. Dr. Elisabeth Soergel

Abstract

This thesis describes an experiment demonstrating Bose-Einstein condensation of erbium atoms in a quasi-electrostatic optical dipole trap. At first the experimental set up will be introduced and underlying physical principles will be explained. Erbium atoms are heat dissociated from macroscopic bulk material in order to create an atomic erbium beam. The atomic erbium beam is slowed down via a Zeeman slower and the decelerated atoms are trapped in a magneto-optical trap. The temperature of the trapped atomic cloud is in the order of a few milli Kelvin and can be further reduced by changing the trapping light's frequency and intensity while ramping the magnetic field gradient down. Afterwards the trapped and precooled erbium atoms are transferred into an optical dipole trap and further cooled by evaporative cooling until a Bose-Einstein condensate was observed. In this thesis the properties of the magneto optical trap are investigated as well as the dynamics of the optical dipole trap which was set up in this thesis. Preliminary results in order to characterise the Bose-Einstein condensate are presented.

Contents

Abstract iii

1 Introduction 1

2 Bose-Einstein condensation and properties of atomic erbium 3
2.1 Bose-Einstein condensation . . . 3
2.2 Erbium - A rare earth element . . . 4
2.2.1 Basic properties . . . 4
2.2.2 Atomic energy spectrum . . . 5

3 Experimental apparatus and methods 7
3.1 Generation and controlling of 401 nm laser light . . . 8
3.2 Generation and controlling of 583 nm laser light . . . 9
3.3 Vacuum system . . . 11
3.3.1 Effusion cell . . . 11
3.3.2 Transversal cooling . . . 13
3.3.3 Zeeman slower . . . 14
3.3.4 Main chamber . . . 17
3.4 Magneto-optical trap . . . 17
3.4.1 Narrow line laser cooling of Erbium . . . 19
3.5 Optical Dipole Trap . . . 21
3.5.1 Erbium atoms in an optical dipole trap . . . 22
3.5.2 Optical dipole trap setup . . . 23
3.5.3 Evaporative cooling . . . 24
3.5.4 Accelerated evaporative cooling . . . 26
3.6 Absorption Imaging . . . 26

4 Procedure - how to create an atomic erbium Bose-Einstein condensate 29

5 Results 33
5.1 Characterisation of the magneto-optical trap . . . 33
5.2 Characterisation of the optical dipole trap . . . 36
5.2.1 Number of Atoms as function of the end power . . . 37
5.2.2 Temperature as function of the end power . . . 37
5.2.3 Trap frequencies as function of the end power . . . 38
5.2.4 Phase space density as function of the end power . . . 40
5.3 Bose-Einstein condensation of erbium . . . 41

6 Outlook 45

Bibliography **47**

A Appendix **53**
A.1 ULE cavity long term drift 53

Danksagung **57**

CHAPTER 1

Introduction

In 1995 the first Bose-Einstein condensates in dilute atomic gases were produced by two groups. The group around W. Ketterle used sodium atoms [1] and the group around C. E. Wieman and E. A. Cornell used rubidium atoms [2] for the first Bose-Einstein condensates. Both groups used alkali atoms since alkali atoms have a relatively simple, hydrogen-like electronic structure. The underlying physics of Bose-Einstein condensation has its origin in work published by A. Einstein in 1905 building on previous work on the quantum statistics by S. Bose. Following early work on the Bose-Einstein condensates of alkali atoms, as described above, also other condensates have been produced, as e.g. with alkaline earth metals like strontium [3], lanthanide elements like ytterbium [4], erbium [5] and dysprosium [6] and even with photons [7].

In order to create a Bose-Einstein condensate in a dilute atomic gas system, free atoms need to be trapped and cooled to temperatures in the Nano-Kelvin regime. Magnetic traps, magneto-optical traps and optical dipole traps showed to be efficient in order to trap and cool alkali atoms. In recent years the more complex atoms as chromium [8], dysprosium and erbium became of interest to researchers due to their high magnetic moment. The strong dipolar relaxation of dense atomic clouds do not allow for the manipulation of a corresponding Bose-Einstein condensate in a magnetic trap; instead optical dipole traps are required for evaporative cooling, as such traps can confine atoms in their minimum energy state.

A further interesting aspect of the lanthanide elements erbium and dysprosium is that they have a non-vanishing orbital angular momentum in their ground states due to missing electrons in their inner atomic energy shells. When using suitable inner shell electronic transitions, a non vanishing orbital angular momentum allows state dependent optical manipulation with large detunings of the driving optical field. In other words the non vanishing orbital angular momentum allows it to prepare quantum states with long coherence times. In contrast, state dependent optical manipulation of alkali atoms can only be done if the used light has a detuning within the fine structure splitting [9]. Elements with a non vanishing electronic orbital angular momentum of the ground state are therefore highly interesting for investigation of frustrated lattices [10] and state dependent entanglement of atoms in optical lattices [11].

The experiment described in this thesis aims to trap erbium atoms in a magneto-optical trap, from which atoms are loaded into an optical dipole trap. Once the atoms are in the optical dipole trap, evaporative cooling is used to increase the phase space density to finally create a Bose-Einstein condensate of erbium atoms. The magneto-optical trap uses a narrow line transition of erbium. The high sublimation temperature of erbium makes it necessary to precool the atoms with a Zeeman slower. This thesis builds up on earlier work [12, 13] where atomic erbium was slowed down in a Zeeman slower and subsequently trapped in a magneto-optical trap. The magneto-optical trap allowed to trap around 10^6 atoms, which

was not sufficient to create a Bose-Einstein condensate via followed evaporative cooling. Therefore the task of this master thesis was it to enhance the number of atoms trapped in the magneto-optical trap followed by setting up an optical dipole trap and implement evaporative cooling which should allow to increase the phase space density until quantum degeneracy.

At the end of August, just at the end of the experimental work of this thesis, a Bose-Einstein condensate of erbium atoms was observed via a transition from a thermal to a bimodal velocity distribution of the atoms. Despite the observation of a BEC this thesis focuses on the characterisation of the magneto-optical trap and the optical dipole trap as well as the necessary experimental setup. However, the measurements done in order to characterise the optical dipole trap also allow to calculate the phase space density of the trapped atoms which can give a numerical confirmation of a Bose-Einstein condensate and will be presented at the end of this work. The data presents preliminary results and will be subject to a more detailed investigation in the PhD thesis of Jens Ulitzsch [14].

CHAPTER 2

Bose-Einstein condensation and properties of atomic erbium

The goal of the experiment is to realise a Bose-Einstein condensate (BEC) with erbium atoms. A BEC is a state of matter in which a macroscopic fraction of atoms with a temperature $T > 0\,\mathrm{K}$ in a system occupies the ground state. Two fundamental conditions must be present: The atoms need to be sufficiently cold and dense. These conditions can be expressed by the phase space density $\rho_{\mathrm{psd}} = n\lambda_{\mathrm{th}}^3$ [15] with n the spatial density and λ_{th} the thermal de Broglie wavelength. The thermal de Broglie wavelength is proportional to $T^{-0.5}$ with T as the temperature. For a free three dimensional atomic cloud the phase space density needs to be equal or greater than $n\lambda_{\mathrm{th}}^3 \geq 2.612$.

In the following chapter the basic theory behind Bose-Einstein condensation will be described. Important properties of the element erbium will be discussed as well as the electronic transitions used for laser cooling in the course of this work.

2.1 Bose-Einstein condensation

In 1924 S. Bose published a paper that was translated by A. Einstein. Bose derived Planck's quantum radiation law by only assuming that the "ultimate elementary region in the phase-space has the content h" [16][17]. Earlier deviations were based on classical statistical mechanics and did not allow solutions which work for the whole spectrum. Einstein extended this idea from photons to identical particles with an integer spin. The underlying statistics is called Bose-Einstein statistics and predicts that for a given set of boundary conditions all particles can occupy the quantum ground state [18].

Non-interacting indistinguishable particles follow the Bose-Einstein statistics

$$N(E) = \frac{1}{\exp\left[\frac{E-\mu}{k_{\mathrm{B}}T}\right] - 1} \tag{2.1}$$

where $N(E)$ particles occupy a quantum state of energy E. Here μ is the chemical potential, k_{B} the Boltzmann constant and T the temperature. To prevent negative occupation numbers the chemical potential μ is chosen that the total number of atoms

$$N_{\mathrm{total}} = \int_0^\infty D(E)N(E)\,\mathrm{d}E \tag{2.2}$$

is conserved. This has the effect that for falling temperatures the chemical potential rises. The limit is set

by $E_0 = \mu$ with E_0 the ground state energy. For small temperatures and $\mu = E_0$ only a limited amount of atoms is in an excited state which results in a macroscopic occupation of the ground state. A macroscopic occupation of the ground state corresponds to a BEC.

An intuitive way of imagining the process is to think of the particles as wave packets with roughly the size of the thermal de Broglie wavelength. The thermal de Broglie wavelength [19],

$$\lambda_{\mathrm{th}} = \frac{h}{\sqrt{2\pi m k_{\mathrm{B}} T}} \tag{2.3}$$

with h the Planck constant and m the mass of the particle, gets longer with falling temperature T. When the wave packets become longer than the average atom-atom distance the wave packets start to overlap and in the case of Bosons[1] form a macroscopic wave packet. These atoms can be described by a macroscopic wave function, which is a striking property of Bose-Einstein condensation. This corresponds to a macroscopic occupation of the ground state. The critical temperature for a square well at which a macroscopic occupation of the ground state is present is given by [20]

$$T_{\mathrm{c}} = \frac{2\pi\hbar^2}{k_{\mathrm{B}} m}\left(\frac{n}{2.612}\right)^{2/3} \tag{2.4}$$

with $\hbar$ the reduced Planck constant and n the spatial density. As can be seen directly the critical temperature is a function of the density. In order to prevent the atoms to interact and to change to a solid state phase a small spatial density is required which result in small critical temperatures of typically a few hundred Nano-Kelvin. As mentioned in the introduction of this chapter the phase space density is defined as

$$\rho_{\mathrm{psd}} = n\lambda_{\mathrm{th}}^3. \tag{2.5}$$

For a free three dimensional atomic cloud the phase space density needs to be equal or greater than $n\lambda_{\mathrm{th}}^3 \geq 2.612$. A three dimensional gas of atoms trapped in a harmonic potential needs a phase space density of $n_0\lambda_{\mathrm{th}}^3 \geq 1.2$ [20] with n_0 the peak spatial density. Details on Bose-Einstein condensation of dilute atomic gases can be found in [20].

2.2 Erbium - A rare earth element

Erbium is a rare earth element which was discovered 1843 by C. G. Mosander. What initially was thought to be pure erbium-oxide turned out to be a mixture of different rare earth metal oxides including erbium, scandium, holmium, thulium and ytterbium. The first basically pure erbium-oxide was produced by two chemists, G. Urbain and C. James, in 1905.

Erbium is to date widely used in optical communication technologies. It allows it to build simple optical amplifiers working in the telecommunication wavelength range of 1530 nm. 1530 nm as wavelength is preferable in optical communications since optical single mode fibres have a low loss rate in this wavelength range. Other transitions make it also suitable for medical applications.

2.2.1 Basic properties

Erbium has the atomic number 68, an atomic mass of 167.26 u and can be found in 6 stable isotopes, ^{162}Er, ^{164}Er, ^{166}Er, ^{167}Er, ^{168}Er, ^{170}Er [21]. All of these isotopes are bosons except the ^{167}Er isotope which is fermionic. For this work we use the ^{168}Er isotope since it has a high abundance and favourable

[1] Bosons are particles with an integer multiple of h.

scattering properties. The ground state electron configuration of erbium is [2][Xe] $4f^{12}6s^2$ [22]. All orbitals are completely filled except the $4f$-shell. This shell misses 2 electrons which leads to an orbital angular momentum of $L = 5$ and a magnetic moment of $7\mu_B$ with μ_B the Bohr-Magneton. Important for this work is also the melting point of erbium since erbium atoms are thermally dissociated from macroscopic bulk material in order to create an erbium atomic beam. The melting point for erbium is 1529 °C.

2.2.2 Atomic energy spectrum

In this work two transitions are used for laser cooling. Figure 2.1 shows the erbium level scheme up to a wave number of 25000 cm^{-1} including the two transition marked by arrows.

The transition driven by a wavelength of 400.91 nm (from now on called 401 nm transition) with its broad line width of (29.7 ± 0.6) MHz [5] is suitable for the Zeeman slower and transversal cooling[3]. Table 2.1 shows the important atomic properties of the 401 nm transition in which one of the $6s$ electrons is excited into a $6p$ state. The remaining $6s$ electron couples with the excited electron to the $^1\mathrm{P}_1$ singlet state.

transition/scattering rate	γ	$1.87 \times 10^8\ \mathrm{s}^{-1}$
lifetime	τ	5.35 ns
natural linewidth	$\Delta\nu_{401}$	29.7 MHz
Doppler temperature[4]	T_D	714 µK

Table 2.1: Spectroscopic data for the transition driven by light at a wavelength of 401 nm used for the Zeeman slower and the transversal cooling. Data from [5, 23]

The transition driven by a wavelength of 582.84 nm (from now on called 583 nm transition) has a narrow linewidth of 190 kHz which makes it usable for narrow line cooling[5]. Also in the 583 nm transition one of the $6s$ electrons is excited into a $6p$ state but in this transition the remaining $6s$ and the excited $6p$ electron couple to a $^3\mathrm{P}_1$ triplet state.

transition/scattering rate	γ	$1.17 \times 10^6\ \mathrm{s}^{-1}$
lifetime	τ	857 ns
natural linewidth	$\Delta\nu_{583}$	0.19 MHz
Doppler temperature	T_D	4.6 µK

Table 2.2: Spectroscopic data for the transition driven by light at a wavelength of 583 nm used narrow line cooling. Data from [23, 24]

[2] [Xe] = $1s^2 2s^2 2p^6 3s^2 3p^6 3d^{10} 4s^2 4p^6 4d^{10} 5s^2 5p^6$

[3] Details on the working principle of the Zeeman slower and the transversal cooling are given in section 3.3.3.

[4] The Doppler temperature will be derived in section 3.3.2.

[5] Details on narrow line cooling are given in section 3.4.1.

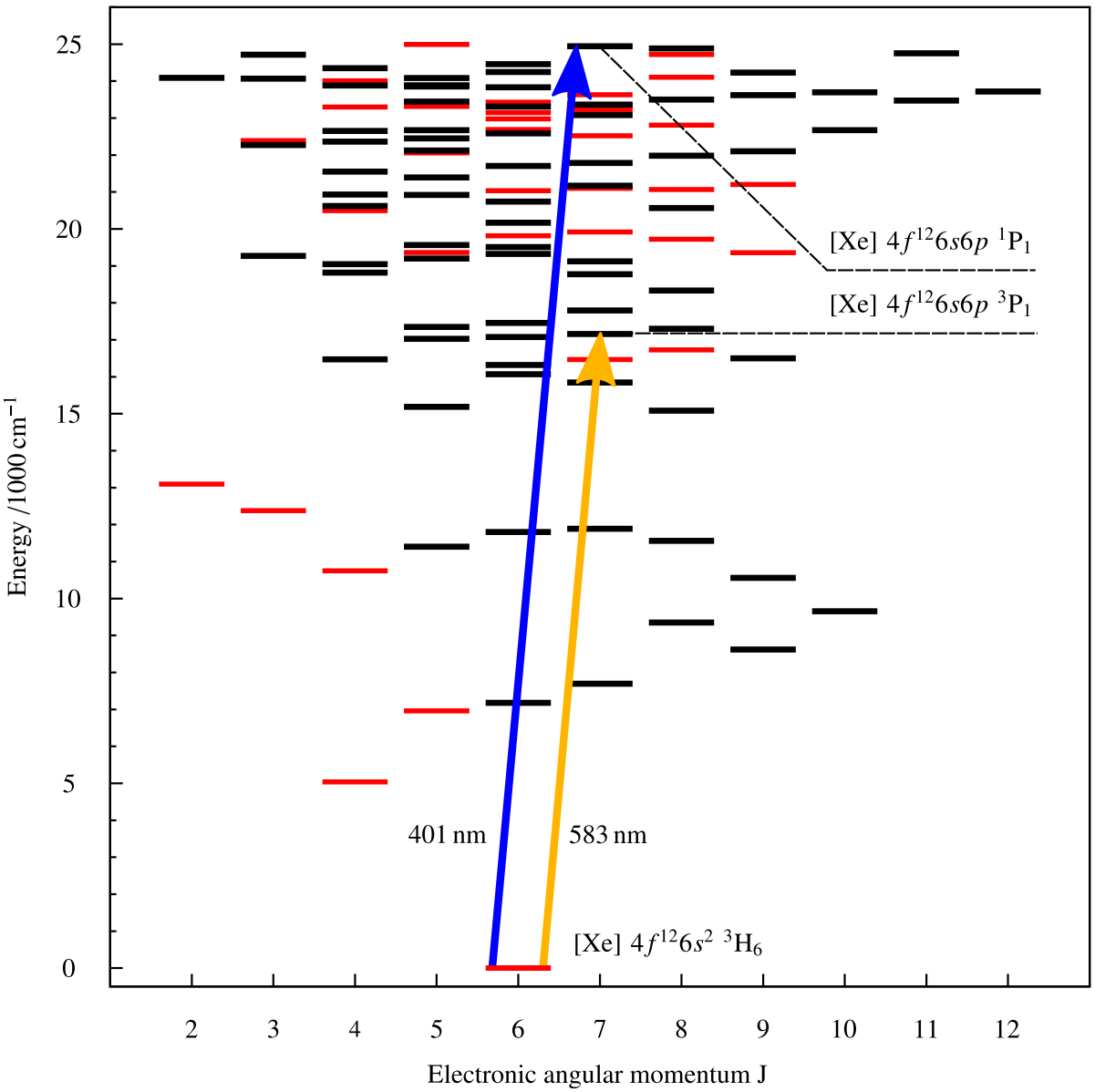

Figure 2.1: Energy level scheme as a function of the total angular momentum J of erbium up to a wave number of 25000 cm^{-1}. The used transitions in this work are marked by arrows. Red lines represent states with even parity. States with an odd parity are represented by black lines. Data taken from [25]

CHAPTER 3

Experimental apparatus and methods

In this chapter the experimental apparatus will be presented. The basic physical principles are discussed and key aspects will be highlighted. The explanations of cooling and trapping mechanisms follow [26] if not differently denoted. A more detailed description of an earlier version of the setup can be found in [13].

Figure 3.1 shows a schematic overview of the experiment. Optical connections between different tables are always realised with fibers.

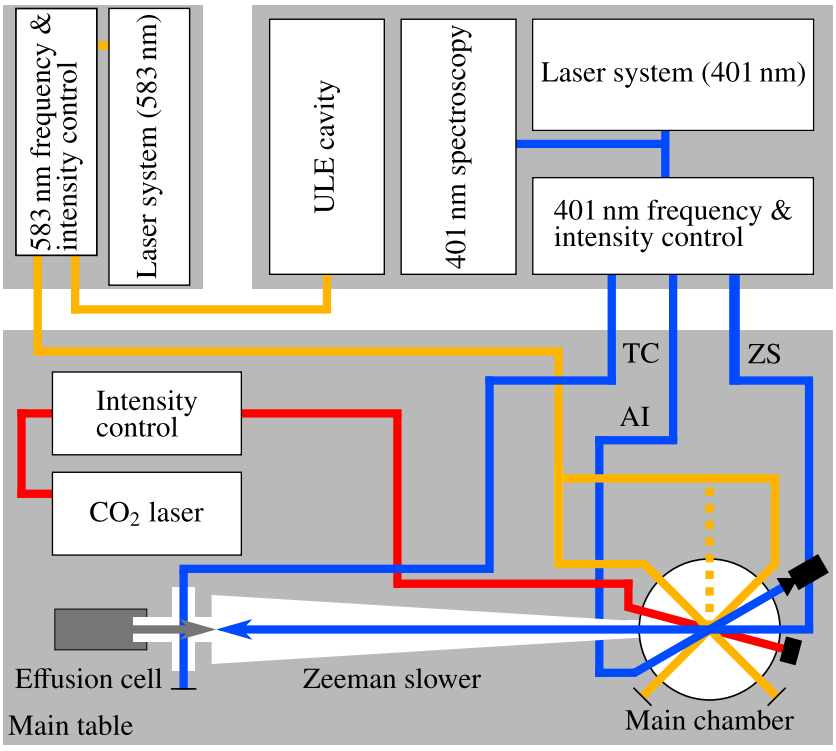

Figure 3.1: Schematic overview of the experiment. The experiment is setup on three optical tables: Two tables for the different laser systems and the main table on which the vacuum chamber, Zeeman slower, effusion cell and CO_2 laser is setup. ZS = Zeeman slower, AI = absorption imaging, TC = transversal cooling.

3.1 Generation and controlling of 401 nm laser light

The system generating the laser light with a wavelength of 401 nm consists out of three parts: The laser, the frequency and intensity control and a spectroscopy setup to stabilise the laser to a certain frequency.

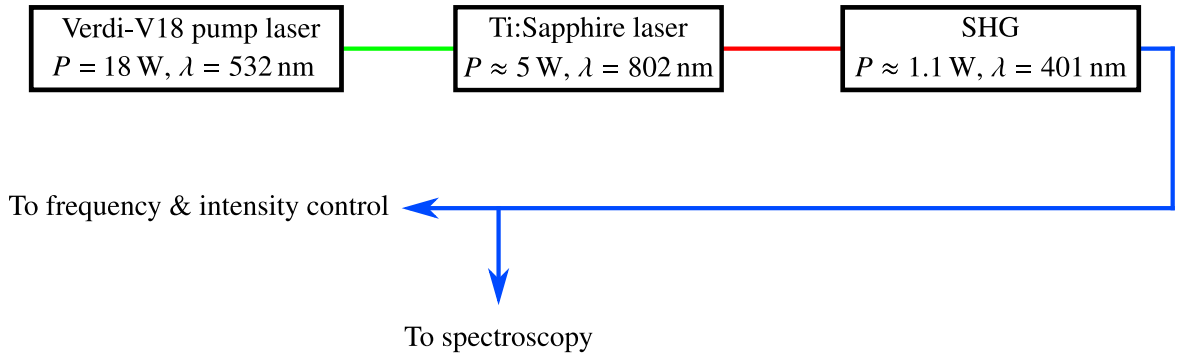

Figure 3.2: Setup to generate the laser light with a wavelength of 401 nm. A pump laser pumps a Ti:Sapphire laser which emits light at a wavelength of $\lambda = 802\,\mathrm{nm}$. This light is frequency doubled to $\lambda = 401\,\mathrm{nm}$ before the beam is split into two parts for the frequency & intensity control and the spectroscopy.

A pump laser emitting light at $\lambda = 532\,\mathrm{nm}$ with a power of 18 W optically pumps a Ti:Sapphire laser which emits light at $\lambda = 801.82\,\mathrm{nm}$ with a power of typically 5 W. This system has an internal locking mechanism which stabilises the frequency relative to a reference resonator to better than a linewidth of 75 kHz. The light is finally frequency doubled by a lithium triborate crystal in a ring cavity to a wavelength near 401 nm with an approximate output power of 1.1 W (see figure 3.2), from now on referred as 401 nm laser light. The second harmonic generation is stabilised using the Hänsch-Couillaud method [27].

The spectroscopy signal (setup shown in figure 3.3) is used to compensate for the long term drift of the reference resonator of the Ti:Sapphire laser. The light passes a double pass acousto optical modulator (AOM) setup which allows it to add a frequency offset with respect to the erbium resonance to the final output of the laser system. After the double pass AOM the light is split into a probe and a pump beam. The pump beam passes an electro optical modulator (EOM) which generates sidebands onto the pump beam before it passes a hollow cathode lamp (HCL) which provides an erbium vapour cloud. The probe beam directly passes the HCL. Both beams are superimposed inside the HCL which results in the case of resonance in a four-wave-mixing process. The photo diode's signal is mixed with the local oscillator signal of the EOM and generates the error signal that is then used to stabilise the laser on the desired erbium resonance. This setup is called modulation transfer spectroscopy [28].

The 401 nm laser light is used for 3 different purposes: The Zeeman slower, the transversal cooling and for absorption imaging. All three applications need different frequencies. The light for the Zeeman slower and the transversal cooling needs to be off resonant whereas the light for the absorption imaging needs to be resonant. Typically the laser is operated somewhere between the different desired wavelengths. Each beam line has an acousto optical modulator (AOM). The diffracted beam is used for the certain application whereas the non diffracted part goes to the next AOM (see figure 3.4). AOMs do not only allow it to modulate the light's frequency but also to switch the light faster than mechanical shutters. The radio signal is turned off and the AOM does not longer diffract the light. Depending on the setup an AOM can diffract a small amount of light without radio frequency signal. The shutters in figure 3.4 serve the purpose to completely block the light.

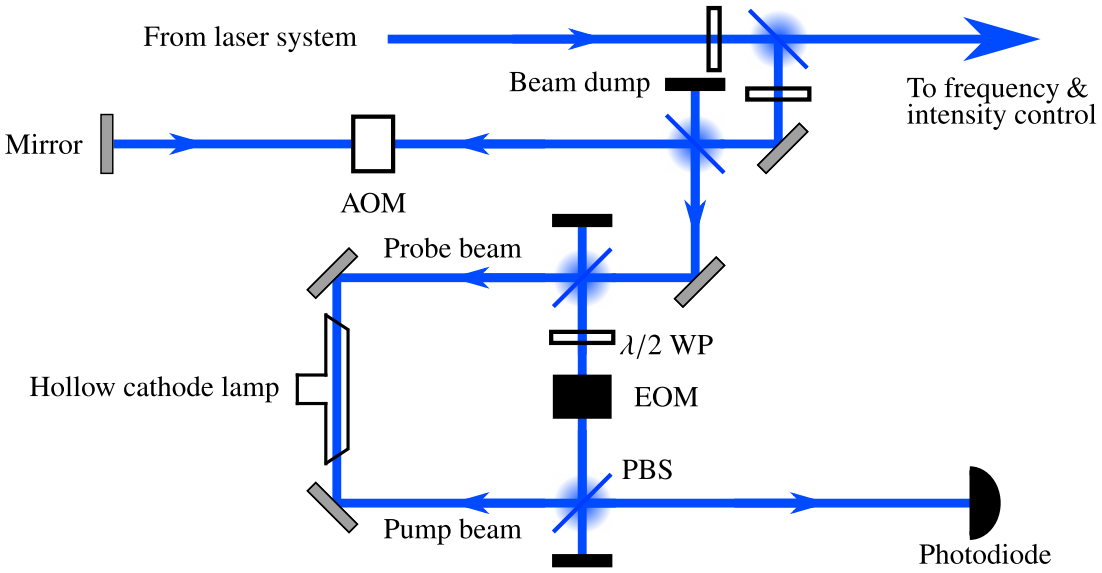

Figure 3.3: Blue spectroscopy setup to generate a modulation transfer spectroscopy signal to externally frequency stabilise the 401 nm laser light. PBS = Polarising Beam Splitter, EOM = Electro Optical Modulator, WP = Waveplate

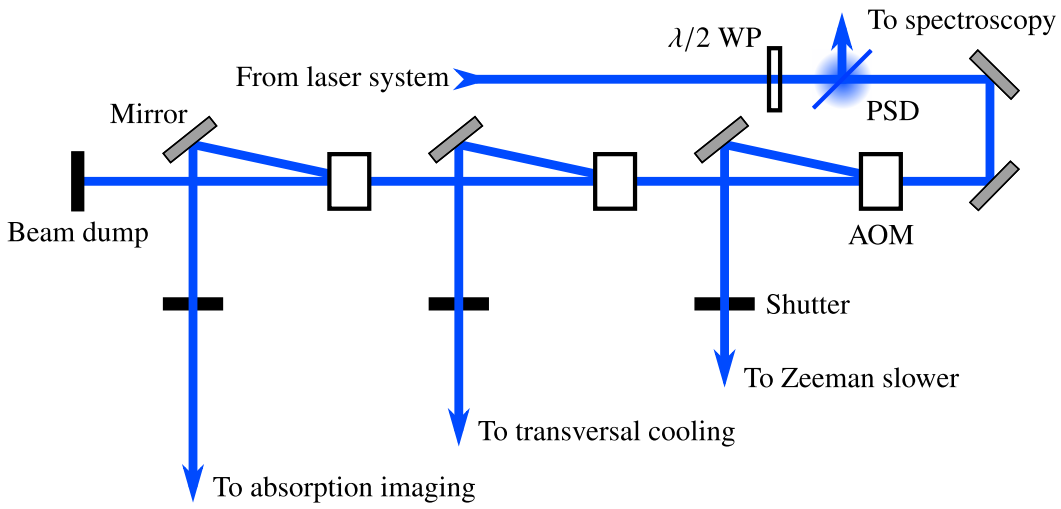

Figure 3.4: Frequency & intensity control setup to generate different beams for the the different applications. The light for the Zeeman slower and for the transversal cooling needs to be off resonant whereas the light for the absorption image needs to be resonant to the atomic transition. The acousto optical modulators (AOM) allow to adjust the frequency and the power of the diffracted light. PBS = Polarising Beam Splitter, WP = Waveplate

3.2 Generation and controlling of 583 nm laser light

Laser light with a wavelength of 583 nm (from now on called 583 nm laser light) is used for the narrow line magneto-optical trap and is generated by a dye laser which is optically pumped by a Verdi-G12 laser. The approximate output power of the dye laser is $P \approx 1.5\,\mathrm{W}$. A detailed description of the dye laser setup can be found in [29].

The MOT procedure which will be explained it section 4 makes it necessary to control the exact

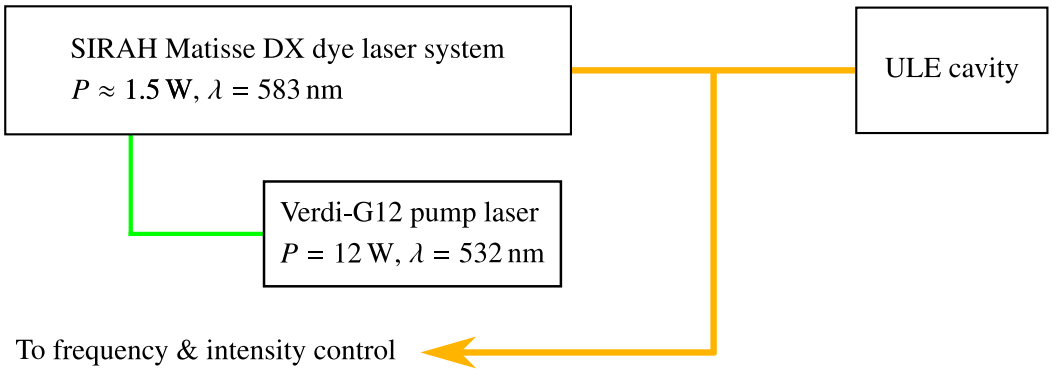

Figure 3.5: Setup to generate the laser light with a wavelength of 583 nm. A dye laser system using Rhodamine 6G dissolved in Ethylene Glycol as dye is pumped by a laser emitting light at a wavelength of 532 nm. The dye laser emits light at 583 nm. The internal frequency stabilisation of the dye laser system is additional externally frequency stabilised by using an ultra-low-expansion cavity lowering the frequency drift of the system to some kHz per day.

wavelength and intensity of the used 583 nm laser light during the experimental sequence. In order to control these parameters the setup shown in figure 3.6 is used. The light passes a double pass AOM setup before being passed to the MOT table. The double pass AOM setup has the advantage that the diffraction angle change caused by a change of the used radio frequency is compensated by a second pass of the AOM. A change of the diffraction angle would change the entry angle and the position of the light beam for following fibres and lower the coupling efficiency into the fibre. A non controllable intensity change during frequency shifts would be the result.

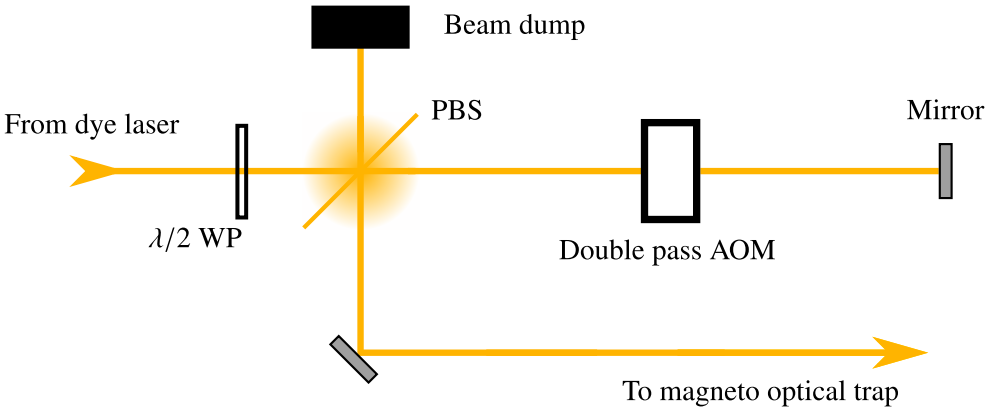

Figure 3.6: Frequency & intensity control setup for the 583 nm laser light. The magneto-optical trap's procedure explained in section 4 makes it necessary to control the frequency and the intensity of the 583 nm laser light used for the magneto-optical trap during the operation of this experiment. AOM = Acousto Optical Modulator, PBS = Polarising Beam Splitter, WP = Waveplate

The dye laser system has an internal reference cavity which allows it to lock the laser within a linewidth of $\Delta\nu_{\mathrm{dye-laser}} < 100\,\mathrm{kHz}$. The long-term drift of the reference cell is in the order of 100 MHz per hour.

The natural linewidth of the used 583 nm transition is $\Delta\nu = 190\,\text{kHz}$. This makes it necessary to add an additional reference cell with a smaller long-term drift. In the experiment an ultra-low-expansion (ULE) cavity is used which has a long term drift in the order of some kHz per day. The long term drift of the ULE cavity is the result of an effect called material creep. The resonator length which is defined by a spacer changes due to relaxation processes in the material. The exact long term drift was desired to be measured in this thesis and could be determined to $(-9.79 \pm 0.01)\,\text{kHz}\,\text{d}^{-1}$. The used method to determine the long term drift is explained in appendix A.1.

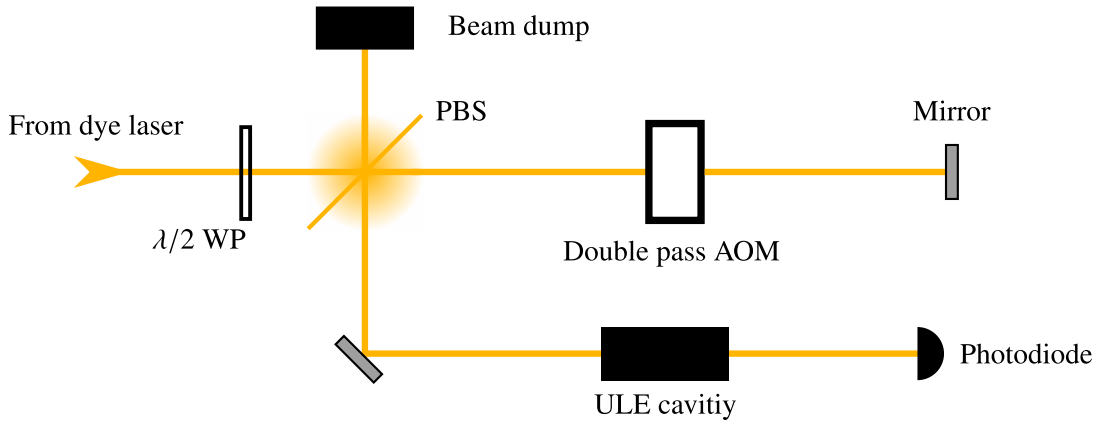

Figure 3.7: Ultra low expansion (ULE) cavity setup for frequency stabilisation of the 583 nm laser light. AOM = Acousto Optical Modulator, PBS = Polarising Beam Splitter, WP = Waveplate

3.3 Vacuum system

The vacuum chamber includes the oven in which the effusion cell is setup, the transversal cooling, the Zeeman slower and the main chamber. The oven and the transversal cooling can be disconnected from the rest of the vacuum system through a valve between transversal cooling stage and Zeeman slower in order to refill the oven without breaking the whole vacuum. Both vacuum segments are pumped using an ion gutter pump whereas the main chamber has an additional titan sublimation pump which can be ignited to enhance the vacuum. During operation the pressure in the oven and in the transversal cooling stage is in the regime of 10^{-8} mbar. The pressure in the Zeeman slower and the main chamber is in the regime of 10^{-10} mbar.

3.3.1 Effusion cell

To thermally dissociate erbium atoms an effusion cell of type DFC-40-10-284-SHE from Createc & Fischer which can achieve a maximum temperature of 1500 °C is used. Inside tantalum heating wires a tantalum crucible is placed. The crucible has two inlets, one with a 3 mm pinhole and the other with a 6.5 mm pinhole to focus the atomic beam. The erbium bulk material is placed inside the crucible in the so called effusion cell (EC) (see figure 3.9). The working temperature here is 1200 °C. The dissociated erbium atoms can escape through a pinhole in the first inlet and enter the hot lip (HL) region. This region has a higher temperature compared to the effusion cell in order to prevent the erbium atoms to condense on the pinholes. Therefore the HL region needs to be hotter than the erbium atoms which escape from

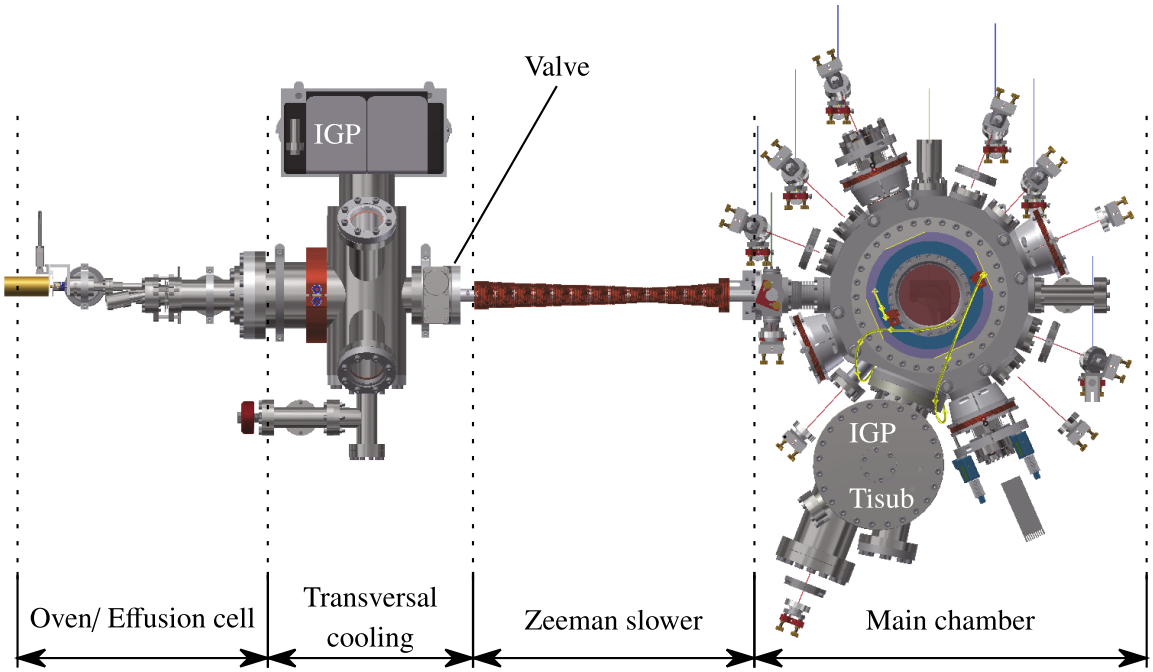

Figure 3.8: Overview of the vacuum system. IGP = Ion Gutter Pump. Tisub = Titan Sublimation Pump

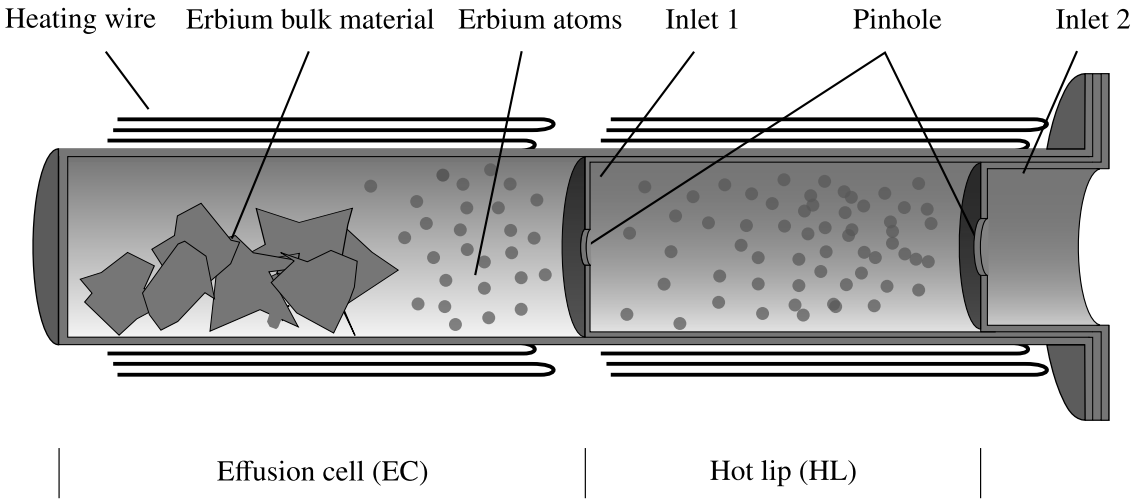

Figure 3.9: Scheme of the tantalum crucible with tantalum inlets and tantalum heating wires. Macroscopic erbium pieces are placed inside the EC. Thermally dissociated erbium atoms enter the HL through a pinhole which has a higher temperature than the EC to prevent the erbium to condense on the walls and the pinholes.

the EC region. The temperature in the HL is 1400 °C. Initially the two pinholes were designed to focus the atom beam and to decrease the evaporation pressure in the HL region. However, measurements by J. Schindler showed that the evaporation pressure is mainly the same in both regions [30]. The divergence angle after the second pinhole is mainly determined by the distance between the second pinhole and the end of the crucible. The RMS velocity of the atoms leaving the effusion cell can be calculated using the average energy of the particles in an ideal gas [31] and derive an expression for the temperature as function of the average velocity $\bar{v}$:

$$T = \frac{m}{3k_\mathrm{B}} \cdot \bar{v}^2. \tag{3.1}$$

This leads to a velocity of roughly $500\,\mathrm{m\,s^{-1}}$ for a temperature of 1400 °C. To be able to close and open the oven it has a mechanical shutter between effusion cell and transversal cooling stage.

3.3.2 Transversal cooling

Directly behind the oven the atoms are transversally cooled to collimate the atomic beam. The underlying principle is called laser cooling and describes the process in which atoms are slowed down by near resonant, red detuned light. From the relation between temperature and velocity given by equation 3.1 it can be seen that a reduction of the velocity corresponds to a reduction of the temperature.

Optical cooling relies on the force applied on particles by photons which is called radiation pressure. An equation for the radiation pressure can be derived by analysing the internal dynamics of a two level atom. The atom has a ground state $|g\rangle$ and an excited state $|e\rangle$ with energy difference $\Delta E = \hbar\omega_0$. Here ω_0 denotes the resonance frequency. An atom at rest can absorb a photon of frequency ω_0 and gets excited. By absorbing a photon not only the energy of the photon is transferred to the atom but also its momentum $|\,\vec{p}\,| = \hbar k$ with k the wave number of the photon. To relax back to the ground state the atom can either emit the photon by stimulated emission or spontaneous emission. In the latter case the photon is emitted in a random direction after the time $\tau = 1/\gamma$ with γ the decay rate respectively the scattering rate. For many absorption events from the same direction and followed spontaneous emission the photons are re-emitted isotropically. The momentum transfers of the emission processes add up to zero and the effective momentum transfers of the absorption and emission processes are determined by the absorption processes.

In the case of stimulated emission the photon is emitted in the direction of the stimulating photon. As result if all cooling photons come from the same direction, no effective momentum is transferred.

Going more into detail a two level system can be described by the optical Bloch equations [26, 32]. The stationary solution for the occupation probability of the excited state ρ_{ee} is given by

$$\rho_{\mathrm{ee}} = \frac{\frac{s_0}{2}}{1 + s_0 + \left(\frac{2\delta}{\gamma}\right)^2} \tag{3.2}$$

with $s_0 = I/I_\mathrm{s}$, $I_\mathrm{s} = 2\pi^2\hbar c/(3\lambda^3\tau)$ the saturation intensity, c the speed of light and λ the light's wavelength. The detuning $\delta = \omega - \omega_0$ of the laser light is given by the difference of the laser light's frequency ω and the resonance frequency ω_0 of the transition. The occupation probability of the ground state is given by normalisation to $\rho_{\mathrm{gg}} = 1 - \rho_{\mathrm{ee}}$. The average force on the atoms, also known as radiation pressure, can be calculated via

$$\vec{F} = \hbar\vec{k}\gamma\rho_{\mathrm{ee}} \tag{3.3}$$

with $\vec{k}$ the wavevector of the light. Together with equation 3.2 the radiation pressure is determined by

$$\bar{\vec{F}} = \frac{\hbar\vec{k}\gamma}{2}\frac{s_0}{1+s_0+\left(\frac{2\delta}{\gamma}\right)^2}. \tag{3.4}$$

This equation is only valid for atoms at rest. Moving atoms will see a Doppler shifted frequency due to the Doppler shift [33]

$$\Delta\omega_{\text{Doppler}} = -\vec{k}\vec{v} \tag{3.5}$$

with $\vec{v}$ the velocity of the atoms. It follows

$$\bar{\vec{F}} = \frac{\hbar\vec{k}\gamma}{2}\frac{s_0}{1+s_0+\left(\frac{2(\delta-\vec{k}\vec{v})}{\gamma}\right)^2} \tag{3.6}$$

A beam of moving atoms can be cooled down by using a counter propagating beam of light which is red detuned ($\delta < 0$). The for several events vanishing momentum transfer of the emission process results in an effective momentum transfer determined by the absorption process in direction of the laser light beam. The mean squared value of the momentum transfer of the emission process does not vanish and heats up the atoms. This limits the temperature to a value greater than zero. The equilibrium temperature, for which the cooling rate and the heating rate are equal, is called Doppler temperature and is given for one dimension by

$$T_{\text{D}} = \frac{\hbar\gamma}{2k_{\text{B}}}. \tag{3.7}$$

The derived equations were made for a two level atom. Interestingly, multilevel atoms can be often cooled to even lower temperatures using so called polarisation gradient cooling, which is a more refined variant of optical Doppler cooling. For elements like the erbium atom with a more complex inner energy structure another effect has to be taken into account. An excited state atom may here decay over several steps into its ground state which may limit the cooling process, e.g. if an atom falls into a state which cannot decay further because it is forbidden by the selection rules. Additional pump lasers can in principle be used to pump those atoms back into the cooling process.

Figure 3.10 shows a schematic drawing of the transversal cooling stage. Optical cooling is realised by driving the 401 nm transition with red detuned light. The broad linewidth of this transition allows it to drive the transition even though the transversal velocity of the atom follows a distribution. The laser light is guided through the atomic beam from four directions and applies an optical pressure towards the centre of the beam. To maximise the cross section of atomic beam and the light beam the light beam is widened up elliptically. The cross section has a size of roughly 1 cm^2.

3.3.3 Zeeman slower

After the transversal cooling stage the atoms enter the Zeeman slower which is constructed out of a double-walled pipe (for cooling purposes) with outer magnetic field coils. The Zeeman slower used in this experiment was designed by M. Rehberger in a previous thesis. Details to the construction process can be found in [34].

A Zeeman slower uses a counter propagating beam of light to slow down a beam of atoms by applying the in equation 3.6 derived radiation pressure onto the atoms. The cooling process is the same process which is described in section 3.3.2. The radiation pressure is only present as long as the light is resonant with an inner atomic transition. In the case of a counter propagating atomic beam the cooling stops as

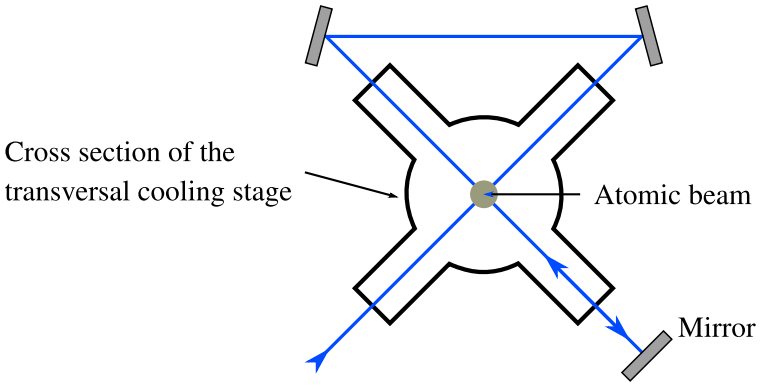

Figure 3.10: Scheme of the transversal cooling setup. The scheme shows the cross section of the transversal cooling stage. The red detuned 401 nm laser light beam is guided through the atomic beam twice before it is reflected and guided back through the atomic beam twice again. This setup applies a force on the atoms towards the centre of the atomic beam to collimate the atomic beam. Since the transversal velocities of the atoms follow a distribution, the broad linewidth of the 401 nm transition is favourable since it allows to excite atoms of a broad range of velocities.

soon as the light is not resonant anymore due to the Doppler shift. In order to keep the cooling process running either the light's frequency needs to change or the inner atomic energy level need to be modified. The latter is favourable since it allows to cool down a whole volume of great expanse at once since the inner atomic energy levels can be modified spatially with a spatial varying magnetic field.

The Zeeman splitting [35] is used to compensate for the Doppler shift and is described by [26]

$$\Delta E_m = m_j \mu_B g_j \mid \vec{B} \mid \tag{3.8}$$

with m_j the magnetic quantum number, g_j the Landé factor and $\mid \vec{B} \mid$ the absolute value of the external magnetic field. To achieve effective cooling the frequency shift caused by Zeeman splitting needs to be equal to the Doppler shift

$$\Delta\omega_{\text{Doppler}} = -\Delta\omega_{\text{Zeeman}} \tag{3.9}$$

$$-\vec{k}\vec{v} = -\frac{\mu_B}{\hbar}(g_{j,e}m_{j,e} - g_{j,g}m_{j,g}) \mid \vec{B} \mid \tag{3.10}$$

$$-\vec{k}\vec{v} = -\frac{\mu_{\text{eff}}}{\hbar} \mid \vec{B} \mid \tag{3.11}$$

The indices "e" and "g" represent the excited respectively ground state of the atom. Basic kinematic theory gives the velocity as function of the position:

$$v(z) = \sqrt{v_0^2 + 2a(z - z_0)}, \tag{3.12}$$

with v_0 the maximum velocity which can be slowed down, a the deceleration parameter and z_0 the point where the deceleration starts. Combining equation 3.11 and 3.12 the desired magnetic field as function of the position is given by

$$\mid \vec{B}(z) \mid = \frac{\hbar k}{\mu_{\text{eff}}} \sqrt{v_0^2 + 2a(z - z_0)}. \tag{3.13}$$

Such magnetic fields can be realised by coils with a spatial dependent number of windings. Since the atoms' velocities follow a distribution not all atoms are decelerated with the same efficiency due to the

Doppler shift. The maximum deceleration is given by $a_{\max} = \hbar k\gamma/(2m)$ and is limited by the finite atomic upper state decay rate.

The Zeeman slower used in this experiment has five independent magnetic field coils in order to be able to tune the magnetic field such that the atoms get slowed down efficiently. A schematic draw of the Zeeman slower can be found in figure 3.11.

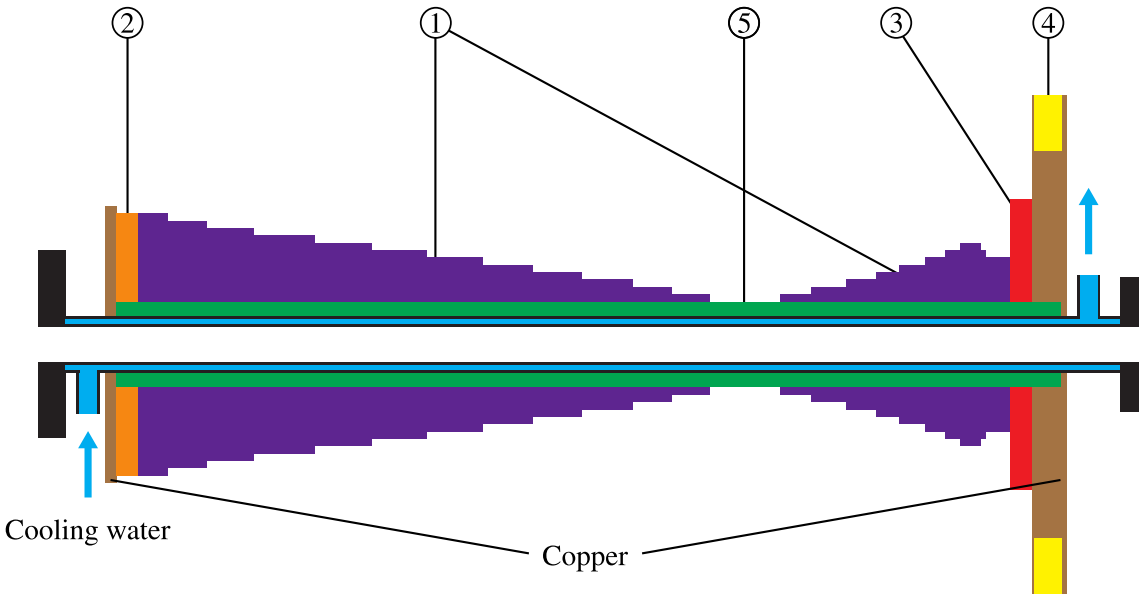

Figure 3.11: Schematic drawing of the Zeeman slower constructed by M. Rehberger. Coil 1 (profile coil) creates a magnetic field with a gradient optimised to shift the inner atomic Zeeman levels such that the decelerated atoms are resonant with the Zeeman slower light. Coil 2&3 are high current coils which are used to control the maximum velocity which is decelerated and to control the outcoupling velocity. Coil 4 with a bigger radius compensates for magnetic fields at the magneto-optical traps position and coil 5 can apply an offset to the total magnetic field which is equivalent to a change of the Zeeman slower light's frequency. Figure taken from [34].

Coil number 1 is the so called profile coil which consist out of 11 segments with different numbers of windings. It provides a magnetic field gradient to compensate for the Doppler shift induced by the cooling process. Coil number 2 is a high current coil which controls the maximum income velocity which can be slowed down. Coil number 3 is as well a high current coil and controls the outcoupling velocity. Coil number 4 is used to compensate the magnetic field at the magneto-optical traps position and coil number 5 adds a constant magnetic field offset. An offset to the magnetic field has the same effect as changing the Zeeman slower light's frequency. The most critical point in the construction of the Zeeman slower is the profile coil. It needs to create the right magnetic field gradient which is determined by the size of the segments. The Zeeman slower uses blue detuned laser light with a wavelength near 401 nm to drive the 401 nm transition, introduced in section 2.2.2. The broad linewidth of this transition is favourable since it allows it to excite atoms with a broad range of velocities and apply a high radiation pressure onto the atoms (see equation 3.6). The relatively high Doppler temperature of this transition is low enough in order to capture the atoms in a magneto-optical trap afterwards. More details on the exact detuning and the applied magnetic fields can be found in [12].

3.3.4 Main chamber

The main chamber is manufactured from stainless steel. Laser beams, for example for the magneto-optical and the optical dipole trap, enter the main chamber via viewports which have anti reflection coatings for the corresponding wavelengths. Additional viewports allow it to install cameras, photomultiplier etc. Magnetic field coils and other important setups installed on the main chamber are explained in the following sections.

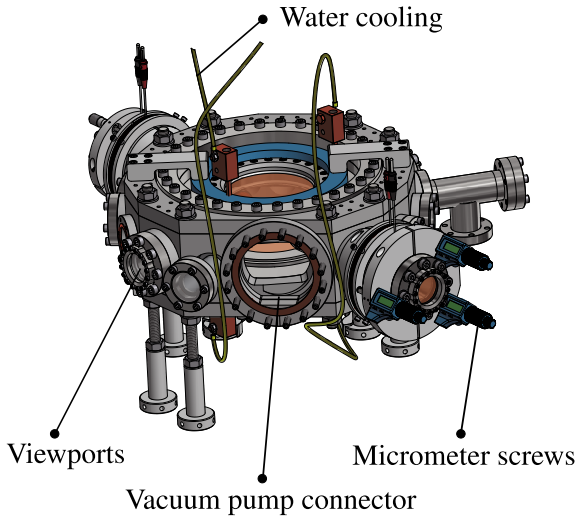

Figure 3.12: Technical drawing of the main chamber. The coils (blue) from the magneto-optical trap are water cooled. The focussing and collimating lens of the optical dipole trap (explained in section 3.5) are attached to micrometer screws. The chambers viewports are anti reflection coated.

3.4 Magneto-optical trap

The by the Zeeman slower decelerated atoms enter the main chamber with a velocity of a few meters per second and are trapped by the magneto-optical trap (MOT). As the name says a MOT uses optical and magnetic effects in combination. In the 1 dimensional case two counter propagating light beams, one right hand circular (σ_+) and the other left hand circular polarised (σ_-), are overlapped. Additional a magnetic quadrupole field is applied in such a way, that in the centre of the system (origin) no magnetic field is present. With rising distance from the centre the linear inhomogeneous magnetic field can be described by $B(z) = Az$.

To describe the total force on the atoms in the MOT (for one axis) equation 3.6 has to be applied from two directions:

$$\vec{F} = \frac{\hbar\vec{k}\gamma}{2}\frac{s_0}{1 + s_0 + \left(\frac{2\delta_+}{\gamma}\right)^2} - \frac{\hbar\vec{k}\gamma}{2}\frac{s_0}{1 + s_0 + \left(\frac{2\delta_-}{\gamma}\right)^2} \tag{3.14}$$

with the detuning given by

$$\delta_\pm = \delta \mp \vec{k}\vec{v} \pm \frac{\mu_{\text{eff}} B}{\hbar} \tag{3.15}$$

and

$$\mu_{\text{eff}} = \mu_B(g_e m_e - g_g m_g) \tag{3.16}$$

the effective magnetic moment for the used transition. Additionally the Zeeman shift due to the inhomogeneous magnetic field needed to be added to the total detuning. It is noticeable that the Zeeman shift and the Doppler shift have opposite signs.

Figure 3.13 shows the situation inside the MOT in one dimension. The lower position line represent the ground state of the atom. The magnetic quantum numbers of ground state and excited state are denoted by m_g and m_e respectively. The red dashed line indicates the frequency of the light beam with δ its detuning with respect to the excited $m_e = 0$ level. An atom inside the MOT will always interact more likely with the beam for which the detuning is smaller, compare δ_- and δ_+ at position z'. The different

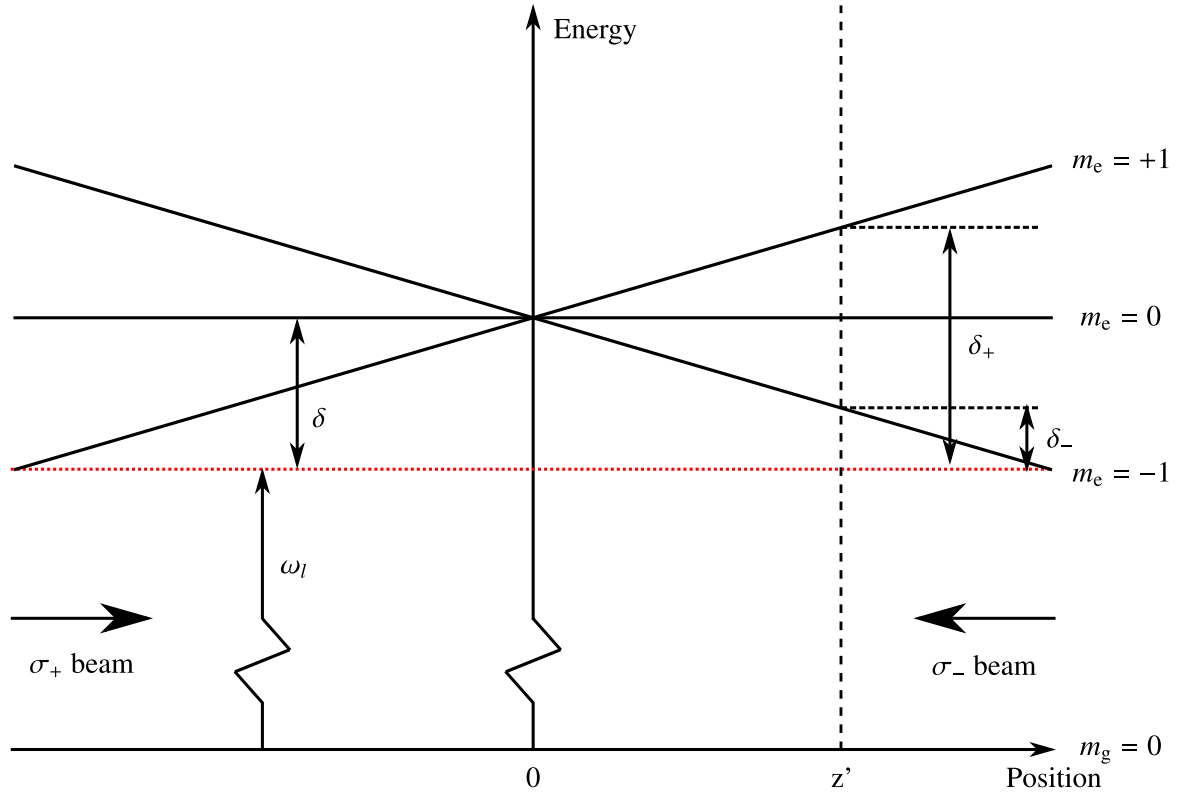

Figure 3.13: Energy scheme inside the MOT for one axis. The red dashed line represents the detuning of the laser light's frequency with respect to the atomic transition. Due to the different circular polarisations and a laser frequency below the atomic resonance atoms moving out of the centre are more likely to interact with the laser beam which drives the atoms back to the centre. The magnetic quantum numbers of ground state and excited state are denoted by m_g and m_e respectively. Figure taken and modified from [26].

detunings are caused by the inhomogeneous magnetic field (Zeeman splitting). Together with the σ_+ and σ_- polarised light an atom inside the MOT is driven towards the centre of the trap. If the detuning is bigger than both the Zeeman and the Doppler shift the force on an atom at position r can be written as the force of a harmonic oscillator

$$\vec{F} = -\beta\vec{v} - \kappa\vec{r} \tag{3.17}$$

with the damping constant

$$\beta = \frac{8\hbar k^2 \delta s_0}{\gamma\left(1 + s_0 + (2\delta/\gamma)^2\right)^2} \tag{3.18}$$

and the spring constant

$$\kappa = \frac{\mu_{\text{eff}} A}{\hbar k}\beta. \tag{3.19}$$

Here A is the magnetic field gradient. The damping rate can be determined as $\Gamma_{\text{MOT}} = \beta/m$ and the oscillation frequency is given by $\omega_{\text{MOT}} = \sqrt{\kappa/m}$. For magnetic field gradients in the order of 10 G/cm such systems are over damped.

3.4.1 Narrow line laser cooling of Erbium

The force acting on an atom in a MOT in one axis (equation 3.14) depends on the laser light's detuning (with respect to the atomic resonance) and the scattering rate of the optical transition. A high scattering rate results in a strong force which is favourable in order to catch atoms but the Doppler temperature will rise linearly with the scattering rate (see equation 3.7). To achieve low temperatures a narrow line transition (small scattering rate γ) can be used. A MOT using a transition with a low scattering rate is often called "narrow line MOT". The dynamics in narrow line MOTs are slightly different to broad line MOTs. Following the dynamics in a narrow line MOT will be discussed shortly following a paper by T. H. Loftus et. al [36].

For a large [1] load detuning δ gravitation needs to be added to the force acting on the atoms inside the MOT in vertical direction

$$\vec{F} = \frac{\hbar\vec{k}\gamma}{2}\frac{s_0}{1+s'+\left(\frac{2\delta_+}{\gamma}\right)^2} - \frac{\hbar\vec{k}\gamma}{2}\frac{s_0}{1+s'+\left(\frac{2\delta_-}{\gamma}\right)^2} - m\vec{g}. \tag{3.20}$$

with $\vec{g}$ the gravitational acceleration and $s' > s_0$ to include saturation effects induced by beams in other directions. The damping coefficient can be derived as

$$\beta = \frac{2\hbar k^2\sqrt{Rs_0 - s' - 1}}{R^2 s_0} \tag{3.21}$$

with $R = \hbar k\delta/(2mg)$. The diffusion coefficient can be derived as

$$D = \frac{\hbar^2 k^2 \gamma}{2R}. \tag{3.22}$$

Taking the ratio of diffusion coefficient and the absolute value of the damping coefficient times the Boltzmann constant the equilibrium temperature can be calculated to

$$T = \frac{\hbar\gamma\sqrt{s_0}R}{4k_B\sqrt{R - s'/s_0 - 1/s_0}}. \tag{3.23}$$

A crucial characteristic value of a MOT is its capture velocity often called critical velocity. The critical velocity for a narrow line MOT can be approximated to [37]

$$v_c = \frac{2\beta d}{m} \tag{3.24}$$

with d the beam diameter.

All calculation to here are all done in the low intensity limit and for one dimension. The low intensity limit describes the case in which the lights intensity is low enough to neglect stimulated emission. As mentioned in section 3.3.2 stimulated emission does not contribute to effective cooling.

The MOT setup shown in figure 3.14 in this experiment uses light from the dye laser system generating the 583 nm laser light. The small natural linewidth (190 kHz) of the 583 nm transition allows it to reach low temperatures of a few Micro-Kelvin in the trapped atomic cloud. The radiation pressure is sufficient

[1] $\delta > \gamma_e$, $\gamma_e = \gamma\sqrt{1+s}$ the power broadened scattering rate

to trap the precooled[2] atoms. Previous work on creating a Bose-Einstein condensate with erbium atoms using the 401 nm transition for the magneto-optical trap showed that the number of loss channels of this transition is too high in order to create an atomic gas of erbium atoms which is cold and dense enough to load it into an optical dipole trap and create a Bose-Einstein condensate via evaporative cooling [12]. The 583 nm transition can only decay into two other excited states, both with low transition rates [38].

The light coming from the dye laser table is widened to approximately 60 mm and then cut to 38 mm by a variable iris. The final light beam has a nearly homogeneous intensity profile compared to the initial Gaussian profile. The light beam is split by two polarising beam splitters and two $\lambda/2$ waveplates into three light beams. Each light beam passes a $\lambda/4$ waveplate before it enters the main chamber. Behind the chamber the light beam passes a second $\lambda/4$ waveplate before being reflected back by a mirror through the setup again. All light beams cross at the centre of the MOT. The intensities in all MOT light beams are the same and are chosen to be well under the saturation intensity. Together with the two magnetic field coils (one on top and the other at the bottom of the chamber) which are operated in anti Helmholtz configuration the light beams induce a three dimensional MOT. Additional three pairs of magnetic field coils operated in Helmholtz configuration allow to add constant magnetic fields in three directions and change the origins position.

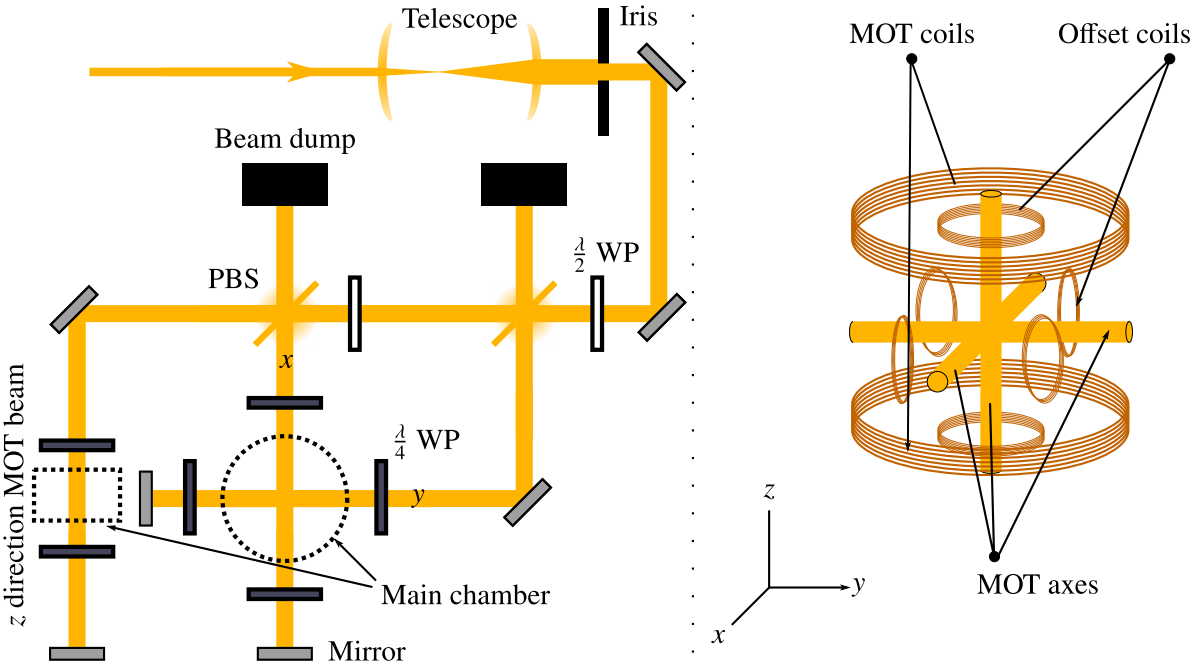

Figure 3.14: **Left:** Scheme of the MOT light's path. A telescope widens the beam to roughly 60 mm and a variable iris cuts it to roughly 38 mm to obtain a nearly homogeneous intensity profile. Polarising beam splitters (PBS) create three beams for the three spatial directions of the MOT. Each beam passes a $\lambda/4$ waveplate (WP), the main chamber and a second $\lambda/4$ waveplate before being retroreflected. All light beams cross in the middle of the MOT. **Right:** Scheme of the six MOT light beams, the 6 magnetic offset coils and the two MOT coils. The offset coils are operated in Helmholtz configuration to add a constant magnetic field whereas the MOT coils are operated in anti Helmholtz configuration to generate a magnetic quadrupole field.

[2] Precooled in the sense that the atoms velocity is decelerated by the Zeeman slower beforehand.

3.5 Optical Dipole Trap

The lowest achievable temperature of an atomic gas trapped in a MOT is limited and described by equation 3.23. The used setup does not allow it to cool the atoms below the critical temperature to create a Bose-Einstein condensate. To cool the atoms to smaller temperatures an optical dipole trap (ODT) using a single focussed Gaussian beam emitted by a CO_2-laser is set up. The CO_2-laser emits laser light at a wavelength of 10.6 µm.

An ODT is based on the inner energy shift in an atom induced by an oscillating outer electromagnetic field called light shift [39]. The first ODT was realised by A. Ashkin [40] trapping micron sized particles and later by S. Chu et al. trapping neutral atoms [41]. The induced shift in a two level atom can be calculated by

$$\Delta E_{\mathrm{g,e}} = \pm \frac{\hbar \Omega^2}{4\delta} \tag{3.25}$$

with $\Omega = \vec{d}_{\mathrm{g,e}}\vec{E}/\hbar$ the Rabi frequency, $\vec{d}_{\mathrm{g,e}}$ the transitions dipole moment and $\vec{E}$ the outer electric field. Since the square of the Rabi frequency is proportional to the intensity of the outer electric field, the energy shift is directly proportional to the intensity. By using red detuned light, i.e. $\delta < 0$, the ground level of the atom is shifted to smaller energies. The energy shift is biggest in the focus which results in a force acting on atoms in their ground state towards the beam focus. The transverse force[3] in the focus is given by

$$F = -\frac{\hbar\gamma^2}{8\delta I_{\mathrm{s}}}\Delta I(r)\left(\approx \frac{\hbar\gamma^2}{4\delta}\frac{I_0 r}{w_0^2}\mathrm{e}^{-r^2/w_0^2}\right) \tag{3.26}$$

whereas the part in the brackets represents the force for a Gaussian beam with w_0 the beam waist in the focus. $I(r)$ is the spatial dependent intensity. The force in longitudinal direction is more complicated but also an attractive force. It is just mentioned that the force due to the light shift is stronger than the radiation pressure induced by spontaneously scattered photons if the detuning is sufficiently large. The radiation pressure decreases with $1/\delta^2$ (see eq. 3.6) whereas the energy shift due to the light shift and with it the resulting force decreases with $1/\delta$.

The trap geometry can be described by the applied potential. The used CO_2-laser emits light in a Gaussian profile. The intensity profile can be described by [42]

$$I(r,z) = \frac{2P}{\pi w^2(z)} e^{-2r^2/w^2(z)} \tag{3.27}$$

with P is the power of the beam and r the radial position around the beam axis z. The beam waist at position z is given by $w(z) = w_0\sqrt{1+(z/z_{\mathrm{R}})^2}$ with $w(0) = w_0$ the beam waist in the focus and z_{R} the Rayleigh length. The Rayleigh length is the length for which the beam's cross section doubled its size. By plugging equation 3.27 into the dipole potential given by [9]

$$U_{\mathrm{dip}} = -\alpha_{\mathrm{static}}\frac{I(\vec{r})}{2\epsilon_0 c} \tag{3.28}$$

with α_{static} the frequency independent static polarisability of the atoms, ϵ_0 the vacuum permitivity and c the speed of light, the traps potential is obtained:

$$U_{\mathrm{dip}}(r,z) = -\frac{\alpha_{\mathrm{stat}}P}{\epsilon_0 c\pi w^2(z)} e^{-2r^2/w^2(z)}. \tag{3.29}$$

[3] Here cylindrical coordinates with r the radial and z the longitudinal component are used

The trap depth U_0 is given by the highest intensity which is at position $z = 0$, $r = 0$:

$$U_0 = -U_{\mathrm{dip}}(r = 0, z = 0) = \frac{\alpha_{\mathrm{stat}} P}{\epsilon_0 c \pi w_0^2}. \tag{3.30}$$

The trap depth can be controlled by the power P of the light beam and the beam waist w_0. The focus' radius of the ODT which is equivalent to the beam waist w_0 can be controlled by the illumination of the focussing lens and can be approximated by [42]

$$w_0 \approx \frac{\lambda f}{\pi w_{\mathrm{l}}} \tag{3.31}$$

with f the focal length, λ the wavelength of the light and w_{l} the illumination radius on the lens.

A dilute gas trapped in an ODT which has an energy noticeable smaller than the trap depth will have a small radial expansion and a small longitudinal expansion compared to the beam waist w_0 respectively the Rayleigh length z_{R}. Doing a Taylor expansion of U_{dip} around $r = 0$ and $z = 0$ up to the second order yields

$$U_{\mathrm{dip}} \approx -U_0 \left\{ 1 - 2\left(\frac{r}{w_0}\right)^2 - \left(\frac{z}{z_{\mathrm{R}}}\right)^2 \right\} \tag{3.32}$$

which is equivalent to a harmonic oscillator in a cylindrical potential

$$U_{\mathrm{harm}} = \frac{1}{2} m \left(\omega_r^2 r^2 + \omega_z^2 z^2\right). \tag{3.33}$$

By comparing equation 3.32 and equation 3.33 the trap frequencies ω_r and ω_z can be determined to [9]

$$\omega_r = \sqrt{\frac{4U_0}{m w_0^2}} \tag{3.34}$$

$$\omega_z = \sqrt{\frac{2U_0 \lambda^2}{m \pi^2 w_0^4}} \tag{3.35}$$

where $z_R = \pi w_0^2 / \lambda$ is used.

3.5.1 Erbium atoms in an optical dipole trap

The used ODT is far detuned and can be described using the quasi-electrostatic approximation. In this experiment the frequency ω of the driving external electromagnetic field is much smaller than any inner electronic transition. The applied external electromagnetic field oscillates slowly and the in the atom induced dipole is driven without phase shift. The atom is behaving like in a static electric field. The dipole potential was already defined in equation 3.28.

The ratio of the photon scattering rate and the trap potential which is a measure for the conservativeness of an ODT is given by [9]

$$\hbar \Gamma_{\mathrm{sc}}(\vec{r}) = 2\left(\frac{\omega}{\omega_0}\right)^3 \frac{\gamma}{\omega_0} U_{\mathrm{dip}}(\vec{r}). \tag{3.36}$$

with Γ_{sc} the photon scattering rate. Typical rates are $\Gamma_{\mathrm{sc}} = 0.001\ \mathrm{s}^{-1}$ [43],[44] and the energy transfer per scattering event E_{trans} is smaller than $k_{\mathrm{B}} \cdot 1\ \mathrm{mK}$ which is smaller than a typical trap depth. The heating

power is defined as [9]

$$P_{\mathrm{h}} = 2E_{\mathrm{trans}}\Gamma_{\mathrm{sc}} \tag{3.37}$$

and is therefore negligible small in case of a quasi-electrostatic ODT [12]. The consequence is that holding times are determined by collisions with remaining thermal gas atoms (background gas) which can be lowered to a minimum by creating a good vacuum. By minimising the scattering rate with background gas typical holding times can reach a few minutes [44].

The dipole potential for atomic erbium can be expressed as [45]

$$U_{\mathrm{edip}}(\vec{r}) = -\frac{I(\vec{r})}{2\epsilon_0 c}\left\{\mathrm{Re}[\alpha_{\mathrm{scal}}(\omega)] + \mathcal{A}\cos\theta_{\mathrm{k}}\frac{M_J}{2J}\mathrm{Re}[\alpha_{\mathrm{vec}}(\omega)] + \frac{3M_J^2 - J(J+1)}{J(2J-1)}\frac{3\cos^2\theta_{\mathrm{p}} - 1}{2}\mathrm{Re}[\alpha_{\mathrm{tens}}(\omega)]\right\} \tag{3.38}$$

with [4] α_i the dipole polarisabilities, [5] $\mathcal{A}$ the ellipticity parameter of the beam, θ_{k} the angle between z-axis and wave vector k, M_J the magnetic quantum number, J the total angular momentum and θ_{p} the angle such that $|\,\vec{e}\cdot\vec{e}_z\,|^2 = \cos^2\theta_{\mathrm{p}}$ where $\vec{e}$ is the unit vector of the polarisation of the light and $\vec{e}_z$ the unit vector in z-direction. Re[x] stand for the real part of a complex number x.

	α_{scal}	α_{vec}	α_{tens}
Re[α_i]	141	−0.084	−2.53
Im[α_i]	1.52×10^{-6}	-0.129×10^{-6}	0.421×10^{-6}

Table 3.1: Polarisabilities for erbium in its electronic ground state with $i \in$ scal, vec, tens in atomic units of $4\pi\epsilon_0 a_0^3$ [12] with a_0 the Bohr radius.

Table 3.1 lists the polarisabilities for atomic erbium in its electronic ground state. As can be seen the scalar polarisability dominates. Since the electro-static ODT approximation holds for the used detuning α_{stat} for the ground state can be determined by comparing equation 3.28 and equation 3.38:

$$\begin{aligned}\alpha_{\mathrm{stat}} &= \mathrm{Re}[\alpha_{\mathrm{scal}}(\omega)] + \mathcal{A}\cos\theta_{\mathrm{k}}\frac{M_J}{2J}\mathrm{Re}[\alpha_{\mathrm{vec}}(\omega)] + \frac{3M_J^2 - J(J+1)}{J(2J-1)}\frac{3\cos^2\theta_{\mathrm{p}} - 1}{2}\mathrm{Re}[\alpha_{\mathrm{tens}}(\omega)]\\ \alpha_{\mathrm{stat}} &\approx \mathrm{Re}[\alpha_{\mathrm{scal}}(\omega)].\end{aligned}$$

Caused by the high magnetic moment such an isotropic behaviour would not be expected. A possible explanation could be the shielding of the filled $6s$-orbital [12]. With the help of the discussed ODT properties and the determination of the static polarisability of atomic erbium in its ground state the trap geometry and trap frequencies can be determined.

3.5.2 Optical dipole trap setup

The setup for the ODT can be seen in figure 3.15. The used CO_2-laser has an output power of $P \approx 120\,\mathrm{W}$ at a wavelength of 10.6 µm. Around one percent of the power is divided out of the beam by a ZnSe[6] plate and is directed through a Fabry-Pérot-Etalon which allows it to check if the laser is running single mode.

[4] scal = scalar, vec = vector, tens = tensor

[5] $\mathcal{A} = 0$ for linear polarised light, $\mathcal{A} = +1(-1)$ for right (left) hand circular polarised light.

[6] Zink selenide

The rest of the light passes an AOM. The AOM runs two frequencies, 30 MHz and 40 MHz respectively, to control the dipole trap's depth by controlling the light's power which enters the main chamber. This is done by changing the amplitude of the 30 MHz signal. If the signal's amplitude is changed the radio frequency (RF) power in the crystal is changed which results in a different diffraction angle (thermal beamwalk). In order to compensate for this change in power and keep the diffraction angle constant the 40 MHz signal is used to keep the RF power inside the crystal of the AOM constant. The thermal beamwalk could significantly reduced by this double radio frequency driving method. The 0th order light beam of the 30 MHz and the 40 MHz signal and the first order diffraction of the 40 MHz signal are directed into a beam dump. The first order diffracted light beam of the 30 MHz signal passes a telescope which allows it to control the light beam's diameter and finally the size of the focus in the chamber (see equation 3.31 to approximate the beam waist in the focus). The change in frequency due to the AOM modulation has no noteworthy influence on the experiment since the ODT is far detuned compared to the erbium resonances. The maximum power in the focus of the ODT is 63 W. Different sizes of the focus were used and the best results in terms of a high phase space density were achieved with a radius of $(23.25 \pm 2.04)\,\mu m$.

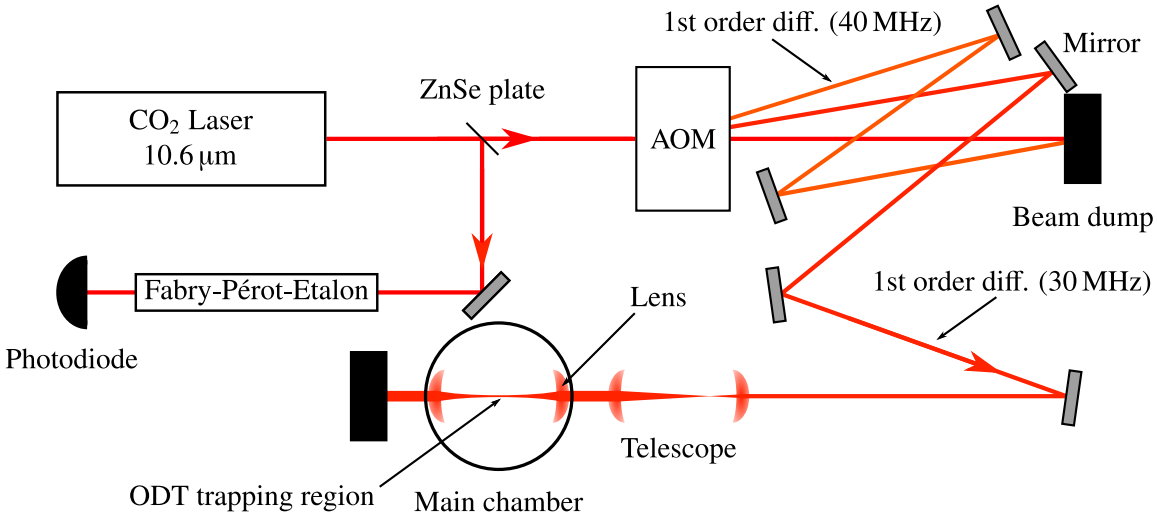

Figure 3.15: Setup for the optical dipole trap. Light emitted by a CO_2-laser passes an AOM which allows it control the light's power inside the main chamber. A second RF signal (40 MHz) on the AOM allows to compensate for thermal diffraction angle shifts. It's diffracted beam is guided into a beam dump. A telescope in front of the main chamber allows it to change the focus size of the light beam inside the main chamber. The maximum power of the trapping beam 63 W. Behind the main chamber the light is blocked by a beam dump.

3.5.3 Evaporative cooling

A dipole trap is a conservative trap and only allows it to trap atoms. To cool the trapped atoms further down it needs an additional cooling mechanisms like evaporative cooling. In fact a dipole trap can even heat up the trapped atoms depending on the photon scattering rate. To prevent heating and keep the photon scattering rate low optical dipole traps can be run far detuned like in this experiment.

The main idea of evaporative cooling which was first realised by N. Masuhara et al. in 1988 for atoms [46] is relatively simple. The trapped atoms' velocities follow a Maxwell-Boltzmann distribution with a mean velocity $\vec{v}$. The mean velocity is decreased by only keeping the low energetic atoms. By decreasing

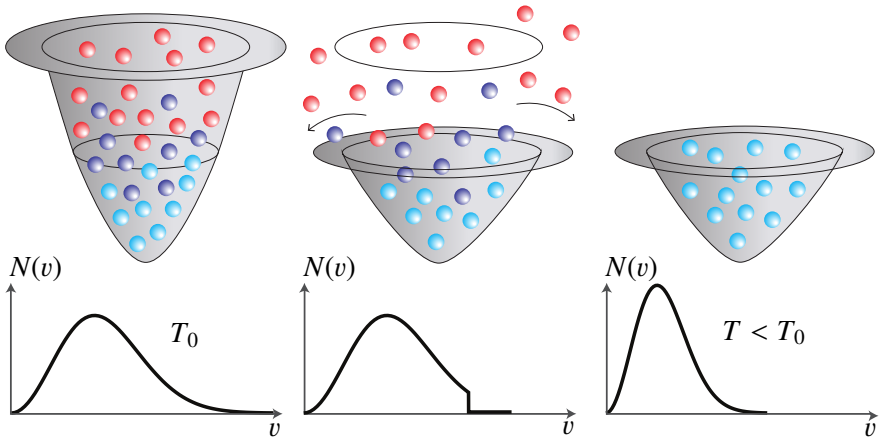

Figure 3.16: Process of evaporative cooling. a) The atoms are trapped in a potential well induced by a far detuned laser. The atoms' velocities follow a Maxwell-Boltzman for temperature T_0. b) The intensity of the laser is lowered which results in a lower potential. The confinement of the potential suffers under evaporation. The hottest atoms (the most energetic ones) can overcome the potential walls and the Maxwell-Boltzman distribution is not longer valid. c) Only the atoms with an energy smaller than the potential walls are still trapped. Collisions between the atoms will restore the Maxwell-Boltzman distribution with temperature T which is below T_0. Figure taken and modified from [34].

the intensity of the light beam the trap depths gets smaller and the highest energetic atoms, the ones with the highest velocities, can get over the potential wall, see also figure 3.16. The Maxwell-Boltzman distribution is no longer fulfilled but will be re-established via collisions between the remaining atoms. This process is called re-thermalisation. For the best possible cooling it is important that the atoms have enough time to re-thermalise because this process shifts the mean velocity to smaller velocities. The time in which the intensity is lowered is crucial. An intensity reduction which is too fast prevents the atoms from re-thermalisation whereas a reduction which is too slow can come in the same order of magnitude as the holding time of the trap, which basically means that the atoms are lost before they are cooled down.

To determine the optimal power ramp the mathematically description starts by defining a parameter $\eta = U_0/(k_B T)$. This ratio should be kept under a value of ten, otherwise evaporation slows down dramatically [47]. The time dependent potential for a constant η can be expressed by [48]

$$U_{\mathrm{dip}}(t) = U_0 \left(1 + \frac{t}{\tau}\right)^{\beta} \tag{3.39}$$

with U_0 the initial potential depth, $\beta = -2(\eta' - 3)/\eta'$, $\eta' = \eta + (\eta - 5)/(\eta - 4)$ and

$$\tau_{\mathrm{e}}^{-1} = \frac{2}{3}\eta'(\eta - 4)e^{-\eta}\gamma_i \tag{3.40}$$

the evaporation rate. The latter is a function of the initial scattering rate γ_i. The initial scattering rate is difficult to determine analytically and is therefore, as well as η, determined in the experiment by optimising the number of atoms trapped in the ODT after

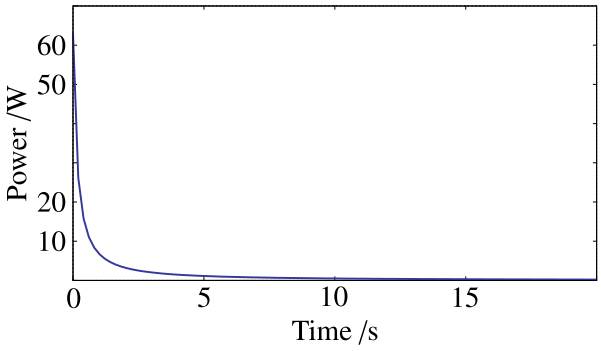

Figure 3.17: Evaporation ramp as used in this experiment with $\eta = 7$ and $\gamma_i = 325$

evaporation. Figure 3.17 shows the evaporation ramp as used in this thesis with $\eta = 7$ and $\gamma_i = 352$. The introduced model does not include scattering with background gas. More details on evaporative cooling can be found in [26] or [49].

3.5.4 Accelerated evaporative cooling

Lowering the potential depth by reducing the light's intensity also reduces the collision rate of the trapped atoms due to the loss of confinement at the trap's bottom. C. L. Hung et al. invented a method which allows it to lower the trap depth while keeping the confinement [50].

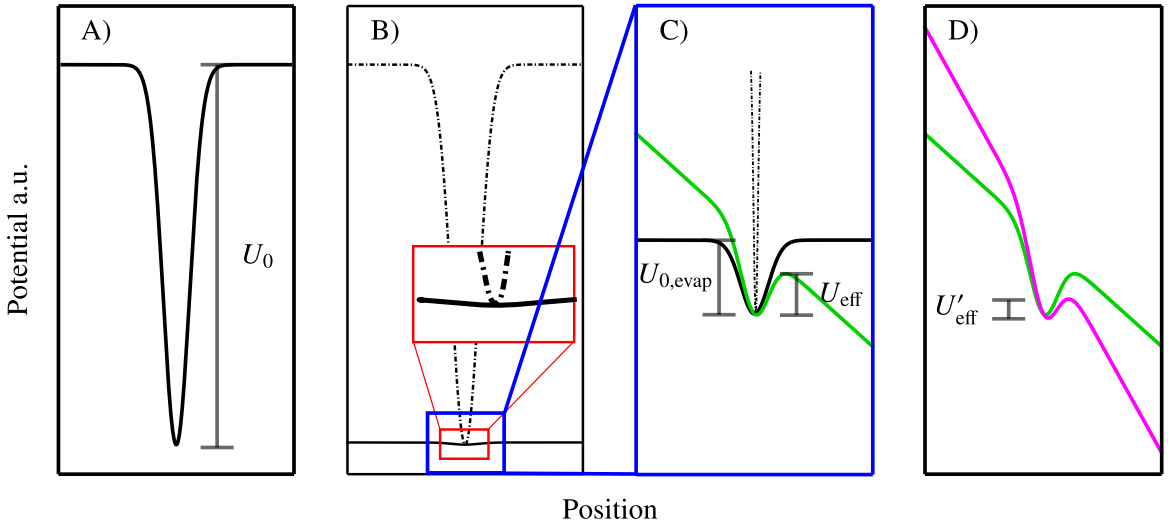

Figure 3.18: Scheme of the accelerated evaporation. **A)** Pure dipole potential with trap depth U_0 at maximum power. **B)** Initial dipole potential at maximum power (dashed line) and dipole potential after evaporation (solid line). The confinement of the trap after evaporation is reduced (see red box). **C)** Dipole potential after evaporation (black solid line) and the sum of dipole and gravitational potential (solid green line). The potential depth $U_{0,\mathrm{evap}}$ is reduced to an effective potential depth U_{eff}. **D)** Sum of dipole and gravitational potential (solid green line) and sum of dipole, gravitational and magnetic potential (purple solid line). The trap depth changes to U'_{eff}. The right outer flank gets steeper and smaller compared to the potential without magnetic field gradient and allows more atoms to escape the trap.

Additional to the ODT potential gravity becomes important for small trap depths. By applying an external magnetic field gradient to the potentials the effect due to gravity can be enhanced, see figure 3.18. The clean dipole potential with trap depth $U_{0,\mathrm{evap}}$ becomes asymmetric due to gravity and the trap depth $U_{0,\mathrm{evap}}$ becomes an effective trap depth $U_{\mathrm{eff}} < U_{0,\mathrm{evap}}$. By applying a magnetic field gradient in direction of gravity the lower flank becomes steeper and smaller which allows it more atoms to escape the trap. In principle the trap depth U_{eff} is lowered to a trap depth U'_{eff} while keeping the light's power constant and with it a better confinement at the bottom of the trap.

3.6 Absorption Imaging

In order to image the atomic cloud an absorption image is taken. The atoms are illuminated with a resonant light pulse (401 nm) directly after all magnetic fields and all light beams are turned off. In this moment the atoms are free. Behind the atom cloud in direction of the light beam a CCD camera is placed

and takes an image of the light beam. Hence the light beam is resonant with the atoms it will be absorbed and partially lost in the image. The image on the camera is a shadow image of the atomic cloud. The intensity for a pixel at position (x, y) is denoted by $I(x, y)$. A second image is taken without the atoms but with the same intensity, same frequency and light pulse length. The corresponding intensity at pixel (x,y) is denoted by $I_0(x, y)$. A dark image $I_D(x, y)$ is taken to determine the background noise. The optical density $D(x, y)$ at pixel (x, y) can be calculated by rearranging Beer-Lambert's law to

$$D(x, y) = -\ln\left(\frac{I(x, y) - I_D(x, y)}{I_0(x, y) - I_D(x, y)}\right). \tag{3.41}$$

Spatial integration of the two dimensional optical density $D(x, y)$ and dividing it by the scattering cross section reveals the number of atoms in the cloud. Figure 3.19 shows a scheme of the setup used for absorption imaging.

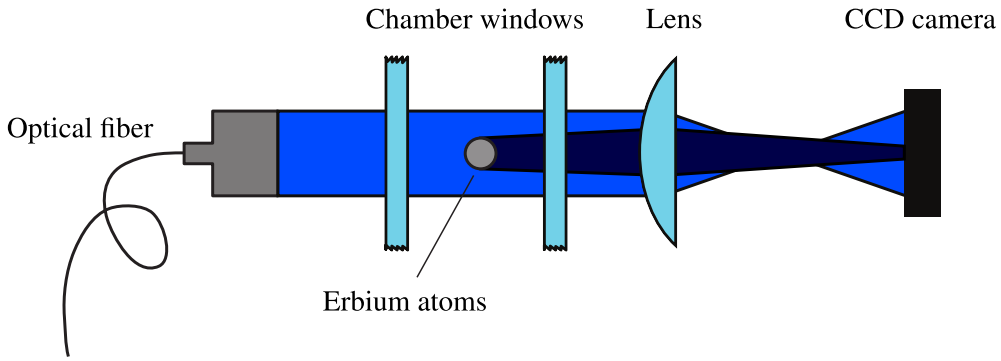

Figure 3.19: Scheme of the absorption imaging setup. The atomic cloud is illuminated with resonant light. The CCD camera takes a shadow image of the atomic cloud. Figure taken from [12].

From an absorption image not only the number of atoms can be determined but also the position in two dimensions and the radius of the cloud. By analysing the radius of the cloud as function of time of free expansion the temperature of the cloud can be determined. Using the position versus time of a spatially oscillating atomic cloud the radial trap frequency can be determined. Details of the methods are given with the corresponding measurements.

CHAPTER 4

Procedure - how to create an atomic erbium Bose-Einstein condensate

This chapter gives an insight into the procedure of the creation of an atomic erbium BEC. The procedure starts with loading the MOT. This phase takes 10 s. During this time the mechanical shutter of the oven is open. The transversal cooling and the Zeeman slower are on as well as the light and the magnetic field gradient of the MOT. Atoms are trapped in the MOT. The MOT light has a detuning of roughly $-33\,\Delta\nu_{583}$ with respect to the transition driven by a wavelength of 583 nm. The broad cooling beam's detuning has an important effect. The atoms trapped in the MOT are pulled down by gravity and are collected in a bowl shaped form below the Zeeman slower light beam (see figure 4.1). This prevents the Zeeman slower of pushing the atoms out of the trap. Furthermore the intersection between atomic beam and trapping region of the MOT is maximised.

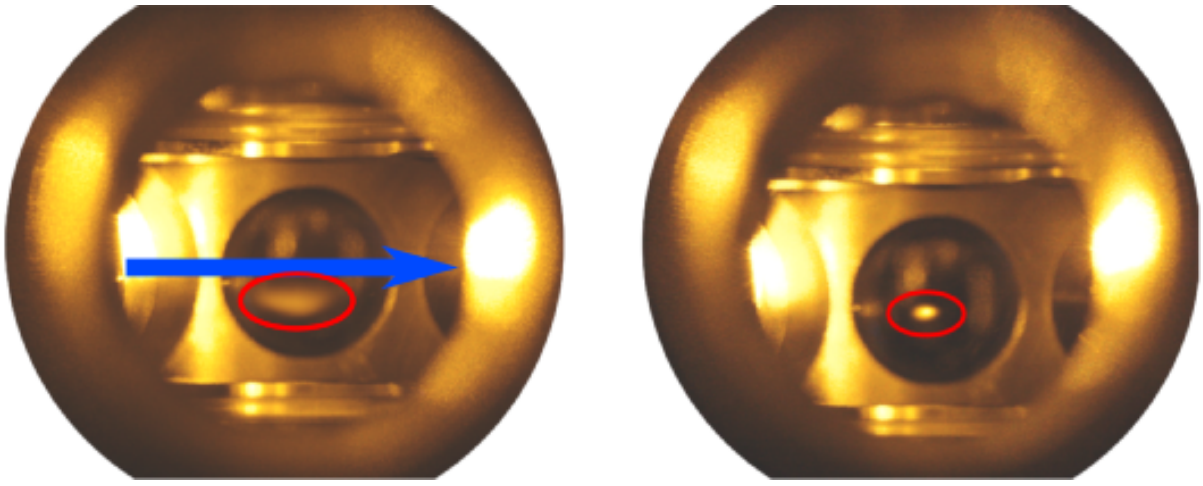

Figure 4.1: **Left:** Picture of the atomic cloud during the loading phase of the MOT. The atoms trapped in the MOT are pulled down by gravity and gather below the Zeeman slower beam (blue arrow) in a bowl like shape. **Right**: Picture of the spatially compressed atomic cloud in the compressed MOT. The atoms are more dense and are lifted up to the centre of the magnetic quadrupole field. The influence of gravity shrinks due to the bigger radiation pressure. Both pictures were taken with an every day's camera by hand and do not show necessarily the moment of maximum loading and maximum compressing.

After 10 s the atomic cloud is spatially compressed by lowering the detuning of the light to roughly $-2.5\,\Delta\nu_{583}$ in 0.2 s. During this phase the transversal cooling and the Zeeman slower are turned off. The

oven is closed by its mechanical shutter. The compressing aims to lower the temperature of the trapped atoms[1] and to prepare the loading into the ODT. In order to maximise the loading efficiency from the MOT into the ODT while minimising the temperature of the atomic cloud the MOT light's intensity and the magnetic field gradient are ramped down during the compressing phase. During the loading phase the intensity in one MOT light beam has a value of $3\,\mathrm{mW/cm^2}$ and is ramped down during the compressing phase to $0.130\,\mathrm{mW/cm^2}$. The magnetic field gradient in z-direction (x, y direction) has a value of $\Delta B_z \approx 3.9\,\mathrm{G\,cm^{-1}}$ $\left(\Delta B_x = \Delta B_y \approx 2.1\,\mathrm{G\,cm^{-1}}\right)$ during the loading phase and is ramped down to $\Delta B_z \approx 1.7\,\mathrm{G\,cm^{-1}}$ $\left(\Delta B_x = \Delta B_y \approx 0.9\,\mathrm{G\,cm^{-1}}\right)$ during the compressing phase. The influence of the MOT light's intensity was analysed by determining the temperature of the atomic cloud as function of the total light power (see section 5.1).

A scheme of the process can be seen in figure 4.2. Start and end values were determined by optimising the number of atoms trapped inside the ODT which is loaded after the end of the compressing phase. The MOT traps in 10 s approximately 5×10^7 atoms. The temperature of the atomic cloud during the loading phase of the MOT is roughly 6 mK[2]. The temperature of the atomic cloud after compressing is approximately 25 µK.

The ODT is loaded by turning off the MOT light and turning on the ODT's light. The magnetic field gradient stays on and stabilises the process[3] (magnetic trap holds atoms in place). Both traps present at the same time would shift the atomic energy levels due to the AC Stark shift to a blue detuning with respect to the light. The atoms would be kicked out of the traps. Figure 4.3 shows an absorption image recorded in the exact moment in which the MOT light is turned off and the ODT trap is turned on. In order to maximise the loading into the ODT the position of the MOT can be changed with offset magnetic field coils (see section 3.4). The loading of the ODT is enhanced by chopping between the MOT and the ODT[4], see figure 4.4. By switching between MOT and ODT both traps are present in the time average picture and a trap similar to a dimple trap is created. The AC stark shift is not as strong and the traps are not destroyed. The optical dipole trap has a maximum trap depth of roughly 2.6 mK. The temperature of the atomic cloud inside the ODT at maximum power was determined to (177.3 ± 2.3) µK and is higher than the temperature of the spatially compressed atomic cloud in the compressed MOT. This heating during the loading phase of the ODT was not further analysed up to now since it did not represented a problem. The temperature is still a lot smaller than the ODT's trap depth. However, this heating will be subject to further investigation in the future. The temperature of the atomic cloud is further reduced by evaporative cooling. After evaporation to 0.8 % of the initial power around 15000 atoms are left with an approximate temperature of 20 nK.

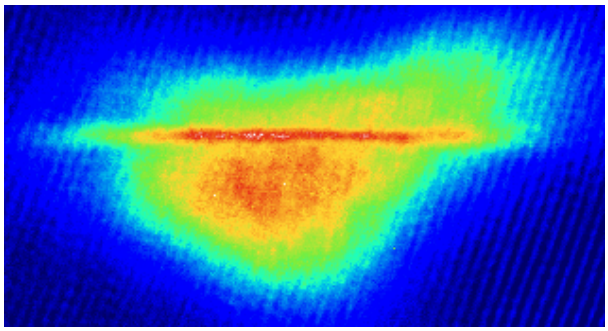

Figure 4.3: Loading of the optical dipole trap. The picture shows an absorption image taken in the moment in which the MOT light was turned off and the ODT was turned on. No cooling beams are present. The atoms still have the form of the MOT due to the inertia of the atoms.

[1] The temperature of the trapped atoms is a function of the light's detuning, see equation 3.23

[2] The temperature of the atomic cloud in the MOT during the loading phase was determined by the "release and recapture" method [51]. The temperature of the compressed atomic cloud will be analysed in section 5.1 by time of flight measurements. The used method will be presented with the corresponding data.

[3] The loading efficiency from MOT to ODT was determined with and without magnetic field gradient. The loading efficiency was higher with magnetic field gradient.

[4] This loading technique was first used in [52].

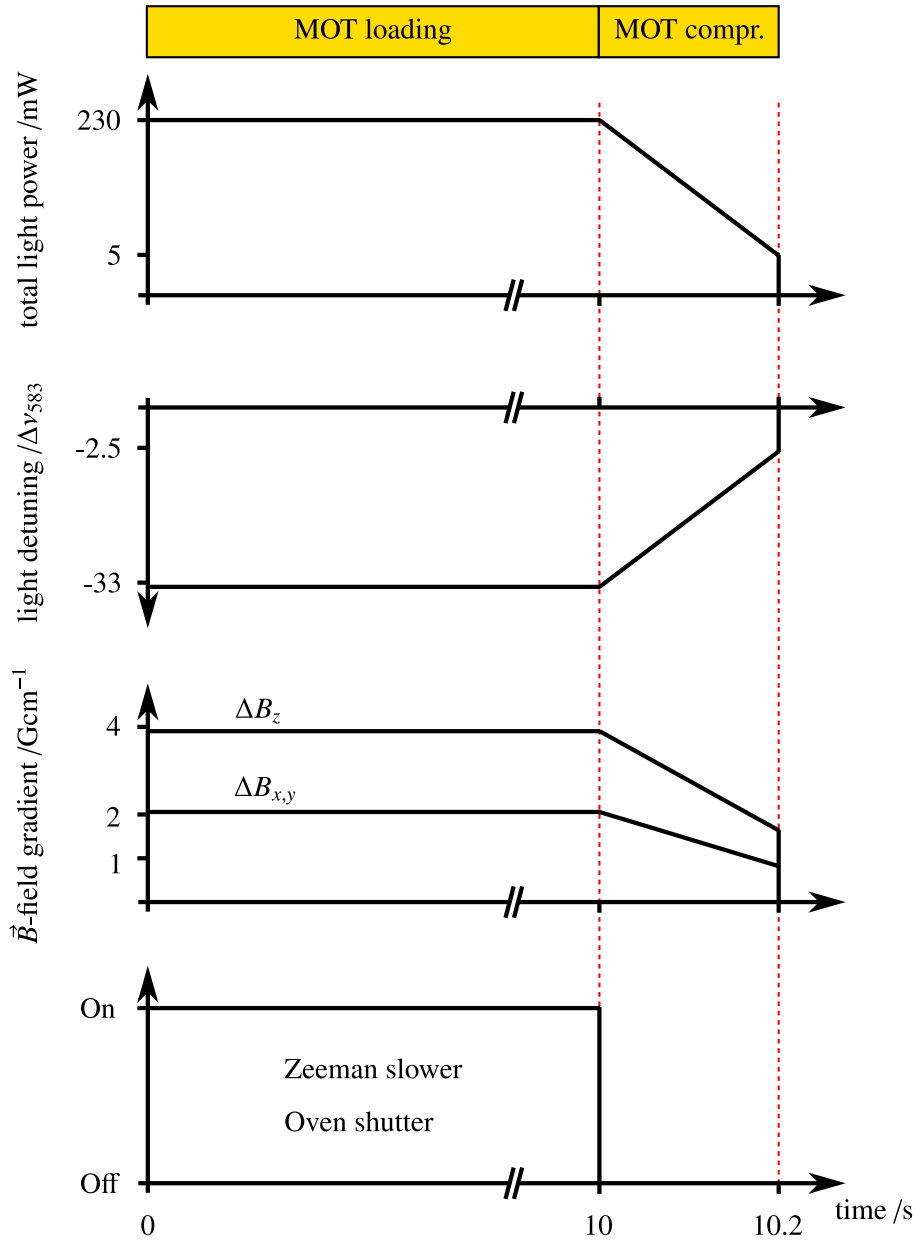

Figure 4.2: Schematic of the temporal sequence of experimental parameters of the MOT during loading and compressing phase. During the compressing phase the MOT light's total power is linearly ramped down from 230 mW to 5 mW. The cooling beams' optical detuning is ramped down from $-33\,\Delta\nu_{583}$ to $-2.5\,\Delta\nu_{583}$ and the magnetic field gradients are reduced by roughly a factor of two. Zeeman slower and oven shutter are on respectively open during the loading phase and are off respectively closed during the compressing phase.

Additionally during all phases constant magnetic fields generated by the offset magnetic field coils of the MOT setup are present to spin polarise the atomic cloud. The magnetic field strengths vary between the phases and are optimised experimentally. This behaviour will also be subject to further investigation in the future.

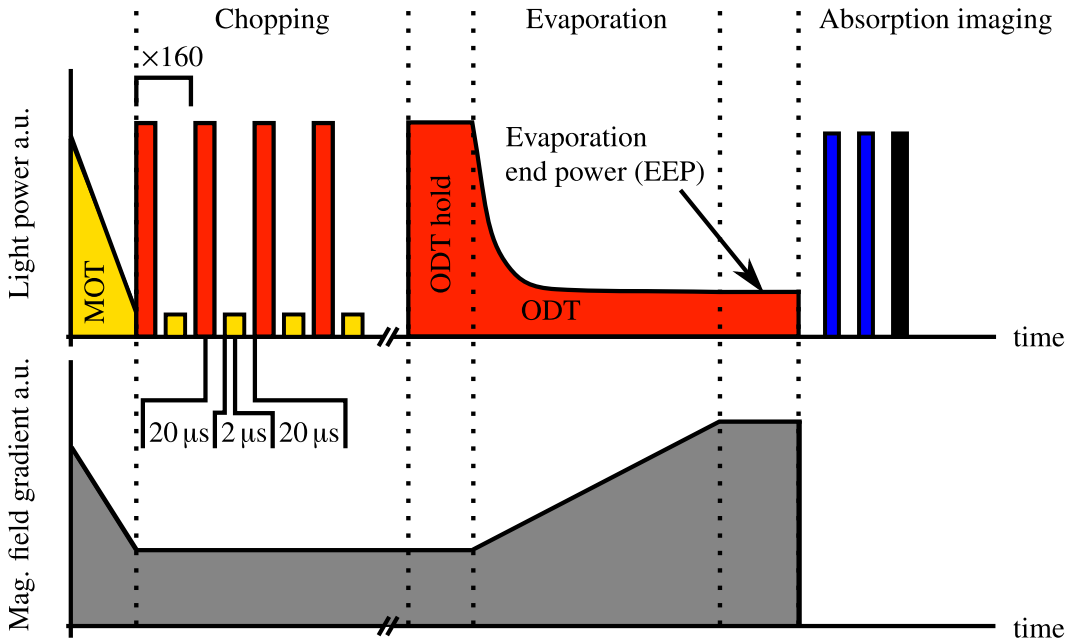

Figure 4.4: Loading phase of the ODT followed by evaporative cooling and the absorption imaging. The MOT light's power is ramped down and finally turned off. The ODT is turned on with full power for 20 µs and turned off again. After 2 µs the MOT is turned on for 20 µs before both traps are off for 2 µs. This process is repeated 160 times and is called chopping method. After the 160 repeats the ODT stays on. The magnetic field gradient which is ramped down during the MOT compressing phase stays constant during the chopping. After the chopping the ODT stays on for 0.1 s before the evaporation starts. During evaporation the light's power in the ODT is ramped down to the evaporation end power (EEP). Parallel to evaporation the magnetic field gradient is ramped up (see section 3.5.4). Depending on the measurement the atomic cloud is hold after evaporation before everything is turned off and the absorption images are taken.

CHAPTER 5

Results

5.1 Characterisation of the magneto-optical trap

To begin with, the magneto-optical trap collecting an ensemble of laser cooled erbium atoms was characterised. This section begins with a measurement of the atomic cloud's radius as a function of the cooling beams detuning.

To load as many atoms as possible from the compressed MOT (cMOT) into the ODT the cMOT needs to be small compared to the loading MOT. The size of the MOT can be controlled with the light's detuning (see figure 3.13). Figure 5.1 shows the measured radius as function of the light's detuning.

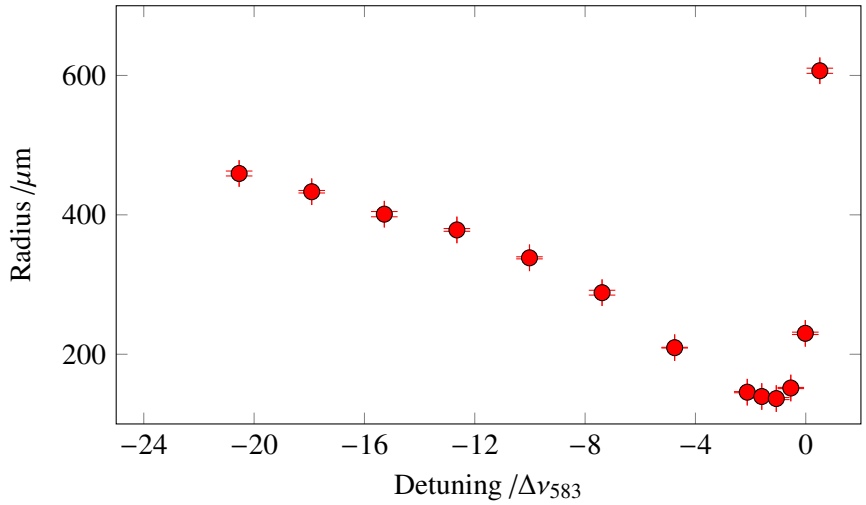

Figure 5.1: Radius of the compressed MOT as function of the MOT light's detuning. For a detuning below approximately $-1\ \Delta\nu_{583}$ the radius begins to grow rapidly due to then being too close to resonance in order to trap the atoms.

It can be seen that the radius shrinks with a shrinking detuning like predicted in section 3.4 but rapidly grows if the detuning gets to small. For a detuning below $-1\ \Delta\nu_{583}$ the detuning becomes too close to resonance in order to trap the atoms. The minimal radius is achieved for a detuning of approximately $-1\ \Delta\nu_{583}$. Next, the dependence of the achieved temperature of the atomic cloud trapped in the MOT on experimental parameters was determined.

Time of flight - measurement of atomic temperatures

The temperature of a dilute gas of atoms can be determined by a time of flight (TOF) measurement. After the atoms are trapped the trap is turned off and the atoms can move freely. The atomic cloud will expand in every direction due to the atoms' velocities and fall down due to gravity. After a time of free expansion (time of flight) an absorption image is taken. This is done several times for different times of flights. From the absorption images the radius of the atomic cloud as function of the time of flight can be determined. Figure 5.2 shows an example TOF measurement of a spatially compressed atomic cloud. The blue line represents the radius evolution as function of time and is defined by

$$r = \sqrt{r_0^2 + \frac{k_B T}{m} t^2} \tag{5.1}$$

with r_0 the initial radius at the time the trap is turned off and t the time of flight. By fitting this function to the measured data the temperature T can be determined [53]. The temperature of the example measurement is determined to $(45.16 \pm 0.19)\,\mu\text{K}$.

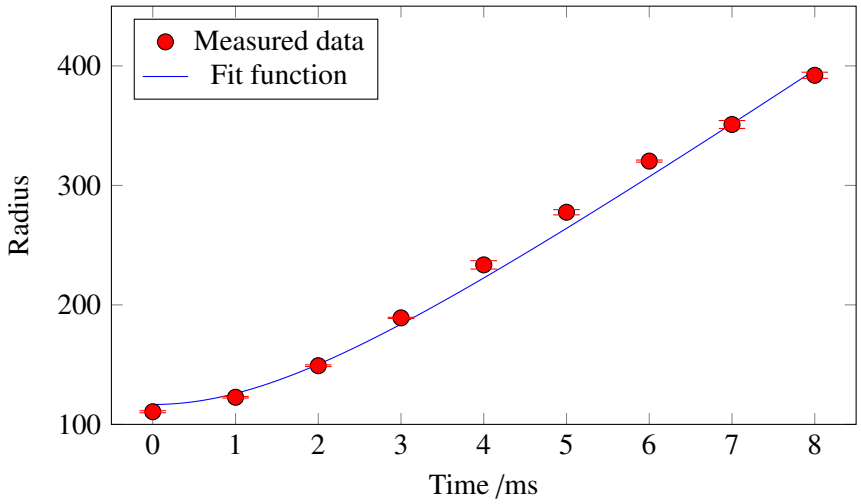

Figure 5.2: Time of flight measurement of a spatially compressed atomic cloud in a MOT with a light detuning of approximately $-1.6\,\Delta\nu_{583}$. The temperature is determined to $(45.16 \pm 0.19)\,\mu\text{K}$ by the blue fit function. The function is defined by equation 5.1.

Temperature as function of the light's detuning

The spatially compressed atomic cloud's temperature as function of the MOT light's detuning can be seen in figure 5.3. For each detuning a time of flight measurement was done. Additionally the number of atoms in the atomic cloud for each temperature measurement is plotted. As expected by equation 3.23 smaller detunings lead to smaller temperatures until the detuning is too small in order to sufficiently cool the atoms. The minimal temperature of roughly $6.5\,\mu\text{K}$ is observed for a detuning of about $-1.5\,\Delta\nu_{583}$. The number of atoms suffers under smaller detunings. A detuning of roughly $-2.5\,\Delta\nu_{583}$ presents a good compromise between temperature and number of trapped atoms.

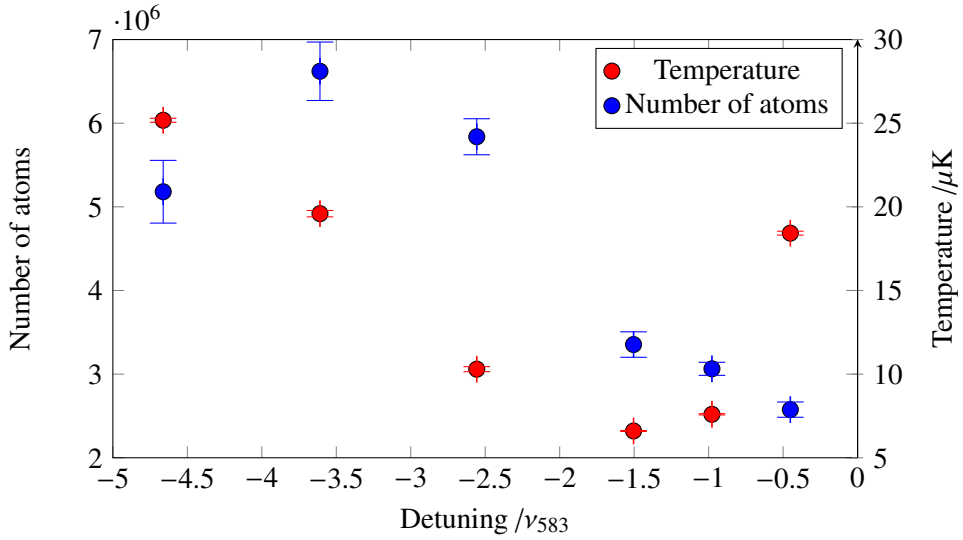

Figure 5.3: Temperature of the spatially compressed atomic cloud as function of the final MOT's light detuning. Smaller detunings lead to smaller temperatures up to a detuning of approximately $-1.5\,\Delta\nu_{583}$. Detunings smaller than approximately $-1.5\,\Delta\nu_{583}$ lead to higher temperatures due to then being too close to resonance for efficient laser cooling. Additionally the number of trapped atoms for the different detunings are plotted.

Temperature as function of the total power

During the compressing of the MOT the intensity of the MOT light is ramped down as described in section 4. The intensity per MOT light beam is proportional to the total power in all beams. Figure 5.4 shows the spatially compressed atomic cloud's temperature as function of the final power in all MOT light beams together. In the used experimental setup it is easier to do a measurement of the temperature as function of the total power since the total power is a variable in the user interface which allows it to control the experimental procedure. A logical dependence can not be observed but less power results in a smaller temperature. For no light at the end of the ramp the MOT turns into a magnetic trap and the behaviour of the atoms change which results in a higher temperature of the atomic cloud. The number of atoms for different powers of the MOT light beams does not show a special dependence. The variation in the number of atoms is in the regime of the normal fluctuations.

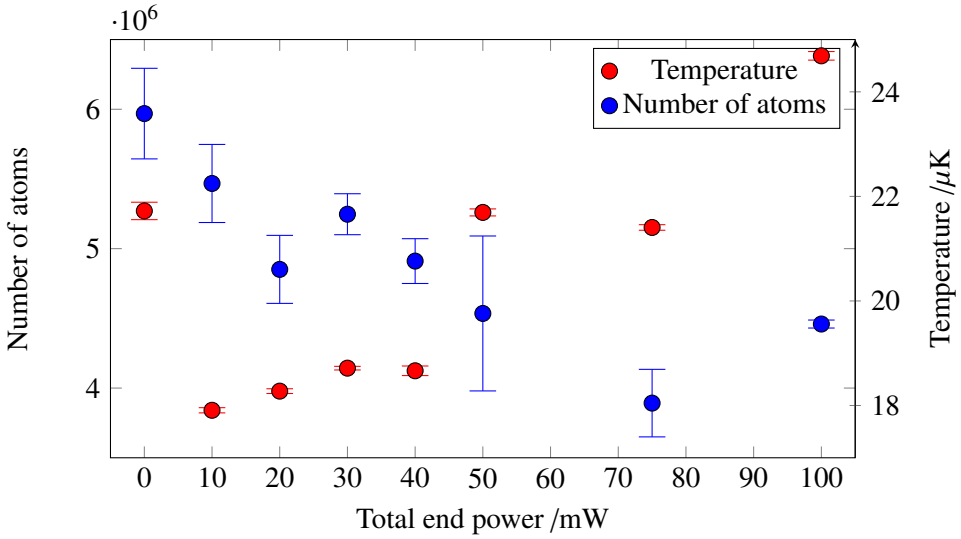

Figure 5.4: Temperatures of the spatially compressed atomic clouds for different end powers of the MOT light beams including the number of atoms for each end power.

5.2 Characterisation of the optical dipole trap

The optical dipole trap is used to cool the atoms further down and to increase the phase space density. Once the phase space density overcomes a value of $\rho_{\mathrm{psd}} \geq 1.2$ a BEC is present. To calculate the phase space density different parameters are needed. The spatial density of an atomic cloud trapped in a Gaussian potential is defined by (in Cartesian coordinates) [9]

$$n(x,y,z) = n_0 \exp\left(\frac{x}{\sigma_x} - \frac{y}{\sigma_y} - \frac{z}{\sigma_z}\right) \tag{5.2}$$

which leads by spatial integration to the spatial peak density

$$n_0 = \frac{N}{(2\pi)^{3/2}\sigma_x\sigma_y\sigma_z} \tag{5.3}$$

with $\sigma_i = 1/(\omega_i)\sqrt{k_{\mathrm{B}}/m}$ and N the number of trapped atoms. The spatial peak density n_0 in the focus is needed to calculate the phase space density defined by equation 2.5 $\left(\rho_{psd} = n_0\lambda_{\mathrm{th}}^3\right)$. Putting equation 2.5, 5.3 and 2.3 together and do a transformation to cylindrical coordinates the phase space density can be determined by

$$\rho_{psd} = \frac{N\omega_r^2\omega_z\hbar^3}{(k_{\mathrm{B}}T)^3} \tag{5.4}$$

with ω_r and ω_z the radial respectively longitudinal trap frequency. The relation between radial and longitudinal trap frequency can be expressed by

$$\omega_z = \sqrt{\frac{\lambda^2\omega_r^2}{2\pi^2 w_0^2}}. \tag{5.5}$$

The following measurements aim to collect the needed information to calculate the phase space density and to characterise the ODT. The number of atoms, the temperatures of the atomic cloud and

the radial trap frequencies are measured for different trapping light powers after evaporation, labelled as "evaporation end power" (EEP). The measurements concentrate on small end powers since the transition from a thermal distribution to a BEC is expected for low temperatures which are achieved by lowering the trap depth (see section 3.5.3).

5.2.1 Number of Atoms as function of the end power

The first measurements determine the number of atoms as function of the EEP. Figure 5.5 shows the evolution of the number of trapped atoms during evaporation as function of the EEP. As expected the number of atoms is reduced by reducing the EEP since with falling EEP also the trap depth gets smaller.

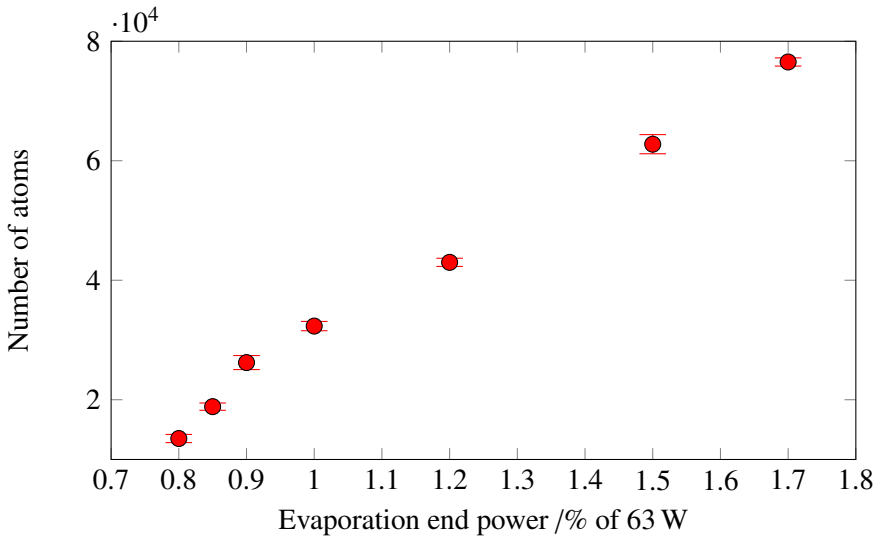

Figure 5.5: Number of atoms in the ODT for different EEPs. The number of atoms falls as expected due to the lowering of the potential's trap depth.

5.2.2 Temperature as function of the end power

The measurement of the number of atoms showed that during evaporation atoms are lost as expected. The next question is if the temperature of the atomic cloud is also reduced by lowering the EEP. The temperature of the atomic cloud trapped by the ODT is determined by a TOF measurement which was introduced and explained in section 5.1. Figure 5.6 shows the temperature development of the atomic cloud in the ODT as function of the EEP. A detailed analysis of the evaporation dynamics and the scaling laws for time-dependent optical traps can be found in [48]. It is mentioned that a linear behaviour between temperature and EEP is expected due to

$$\frac{T(t)}{T_\mathrm{i}} = \frac{U_\mathrm{dip}(t)}{U_\mathrm{dip,i}} = \frac{P(t)}{P_\mathrm{i}} \tag{5.6}$$

with the indices "i" labelling the initial value of the corresponding quantity. The linear fit in figure 5.6 describes in good accordance the measured data. In order to characterise the cooling efficiency it is useful to plot the temperature of the atomic cloud as function of the atom number in the atomic cloud as shown in figure 5.7. For higher atom numbers (higher EEPs) the relation between temperature and number of atoms is linear which speaks for an efficient cooling. For smaller atom numbers the trend flattens

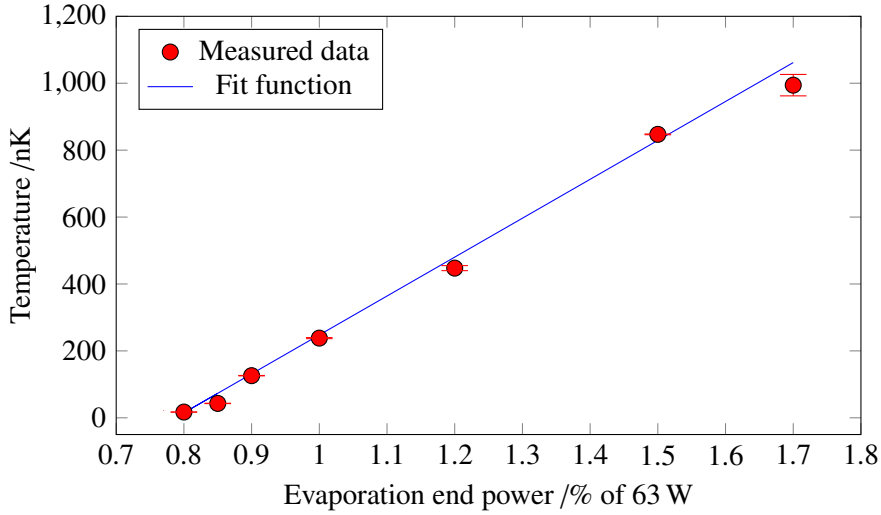

Figure 5.6: Temperature of the atomic cloud in the ODT for different EEPs. The temperature falls linearly with falling EEP as expected by equation 5.6.

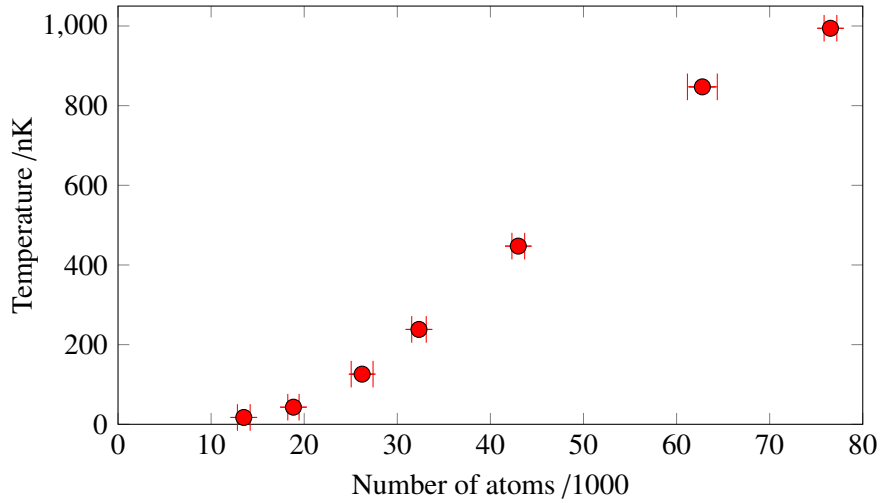

Figure 5.7: Temperature of the atomic cloud as function of the number of trapped atoms. For higher atom numbers (higher EEPs) the relation between temperature and atoms trapped is linear. For smaller EEPs the linear behaviour flattens out which shows that the cooling efficiency of the evaporation process is not optimal and needs further optimisation for small EEPs.

which means that the cooling efficiency for smaller EEPs goes down. By changing the parameters of the evaporative cooling the cooling efficiency should be able to get enhanced. Probably it would be efficient to split the evaporation ramp described in 3.5.3 into two parts and use two different ramps for different regimes. However, for the moment figure 5.7 shows that the cooling process works.

5.2.3 Trap frequencies as function of the end power

As seen in equation 5.4 the trap frequencies are of interest. In this experiment the so called breathing method (scheme in figure 5.8) was used to measure the radial trap frequency. After evaporation the trap

is turned off for 50 to 100 µs. In this time the initially trapped atoms are accelerated by gravity and fall down before the trap is turned on again. After that absorption images for different holding times t_h in the order of a few microseconds are taken. The atomic cloud trapped again in the ODT still has the gained energy due to the free fall and sloshes in the dipole potential. The evolution of the atom cloud's position can be determined as a function of the holding time and follows a harmonic oscillation with the radial trap frequency ω_r which allows it to fit a cosine function of the form $p(t) = A\exp[-t/\tau]\cos(2\pi\nu_r t + \phi) + p_0$ with $2\pi\nu_r = \omega_r$ onto the data and determine the radial trap frequency. Figure 5.9 shows a typical breathing

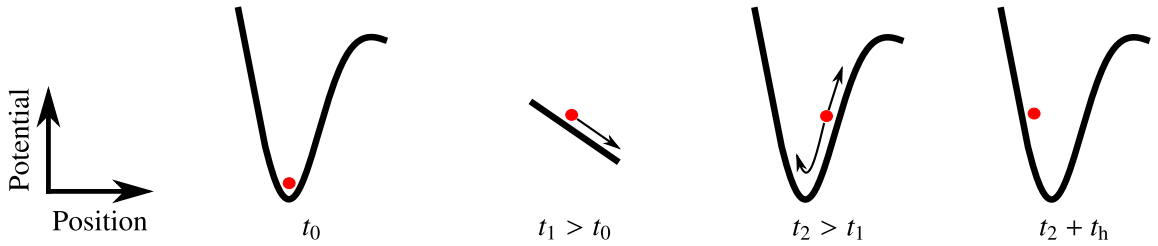

Figure 5.8: Scheme of the breathing mode measurement. The red dot represents an example atom. **t_0:** The atom is trapped in the potential and moves freely inside the potential. **t_1:** The trap is turned off and the atom is accelerated by gravity and gains energy. **t_2:** The trap is turned on again. The atom is trapped again and sloshes around due to the gained energy. **$t_2 + t_h$:** After a holding time t_h the position of the atom is determined by an absorption image.

mode measurement with fit function. Figure 5.10 shows the radial trap frequencies for different EEPs. Due to equation 3.34 a square root function is expected. The blue line in figure 5.10 represents equation 3.34 with $w_0 = (23.25 \pm 2.04)$ µm. The measured radial trap frequencies fall down faster than expected by equation 3.34 as attributed to the influence of gravity and the magnetic field gradient which are not included in the model used to derive the analytical expression of ω_r.

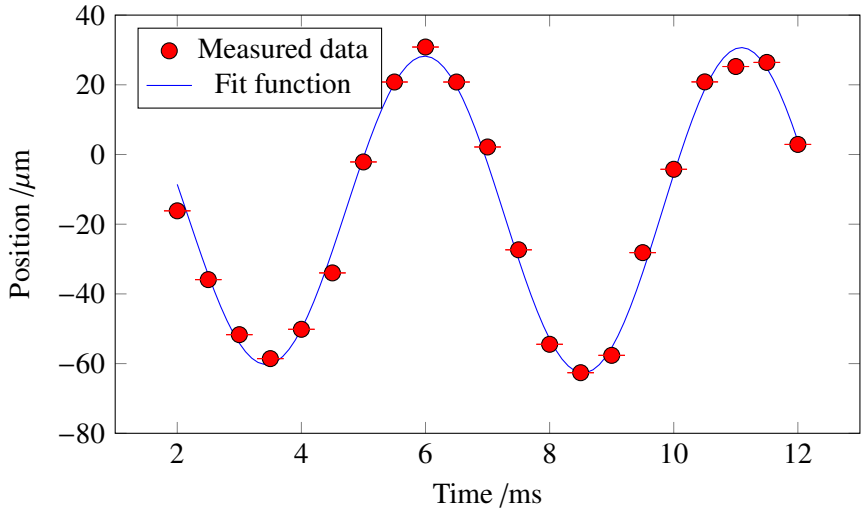

Figure 5.9: Example of a trap frequency measurement with $\omega_r = (197.6 \pm 1.2)$ Hz. The position of the cloud is measured for different holding times. The blue function has the form $p(t) = A\exp[-t/\tau]\cos(2\pi\nu_r t + \phi) + p_0$ with $2\pi\nu_r = \omega_r$.

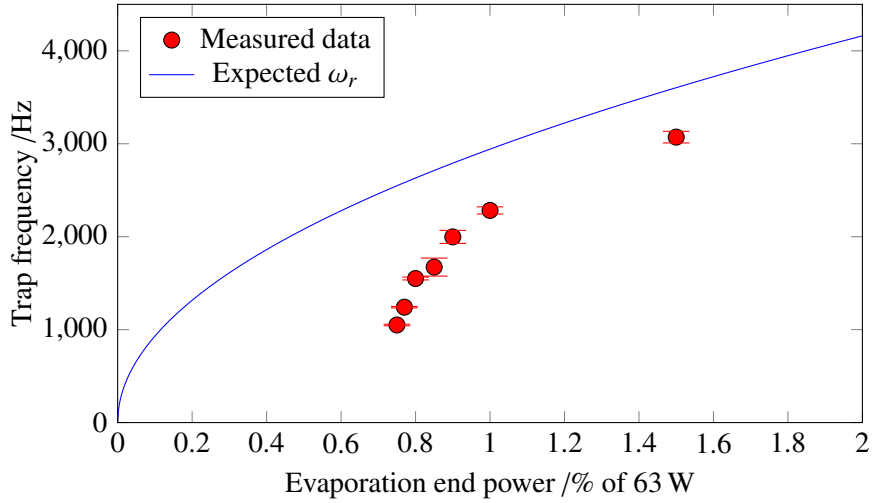

Figure 5.10: Trap frequencies as function of the EEP. The blue line represents equation 3.34 with $w_0 = (23.25 \pm 2.04)\,\mu m$. The model used to derive equation 3.34 does not include gravity and a magnetic field gradient is understood to cause the difference between measured data and equation 3.34.

5.2.4 Phase space density as function of the end power

From the measured data the phase space denisty can be calculated as function of the EEP. The results are shown in figure 5.11 and the corresponding data can be seen in table 5.1. The data shows that for EEPs below 0.85 % of the initial power the necessary phase space density to be clearly quantum degenerated is reached. The phase space density overcomes the critical value of 1.2 between 0.9 % and 0.85 % of the initial power.

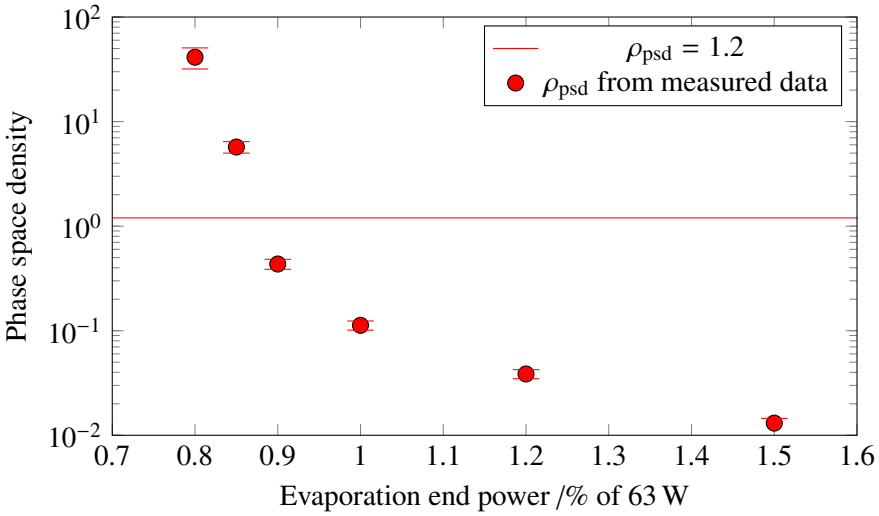

Figure 5.11: Calculated phase space densities as function of the EEP. The data can be found in table 5.1. The critical phase space density of 1.2 is exceeded during evaporation between 0.9 % and 0.85 % of the initial power.

From table 5.1 it can be seen that quantum degeneracy is reached with less than 20000 atoms. In order to reach quantum degeneracy with less than 20000 atoms the atoms need to be sufficient cold. The temperature has to be smaller than approximately 100 nK.

P_{End} /% of 63 W	ν_r /Hz	Temperature /nK	Number of atoms	ρ_{psd}
0.80	126 ± 3	17.2 ± 0.2	13509 ± 684	41.273 ± 9.408
0.85	146 ± 3	43.0 ± 0.5	18843 ± 607	5.712 ± 0.716
0.90	162 ± 4	125.9 ± 0.6	26221 ± 1174	0.434 ± 0.047
1.00	182 ± 5	238.2 ± 1.6	32328 ± 779	0.113 ± 0.011
1.20	218 ± 6	447.4 ± 7.5	42997 ± 684	0.039 ± 0.004
1.50	253 ± 7	847.2 ± 1.1	62771 ± 1603	0.013 ± 0.001

Table 5.1: Calculated phase space densities and the corresponding measured data. The critical phase space density of 1.2 is exceeded during evaporation between 0.9 % and 0.85 % of the initial power.

5.3 Bose-Einstein condensation of erbium

An atomic erbium Bose-Einstein condensate was first observed in our group on the 29th of August 2016. Figure 5.12 shows a time of flight measurement after evaporation. The time between each picture is 2 ms. After 14 ms the cloud is round and following pictures show a radius inversion. The radius inversion is not a result of the cloud's temperature but a consequence of the repulsive forces between the atoms in the BEC. The trapping force in radial direction is stronger than the force in longitudinal direction due to the traps geometry. In equilibrium the forces are counterbalanced by the repulsive forces between the atoms. Using mean field theory it can be shown that the short axis has a larger energy gradient. Instantaneously switching off the ODT leads to a faster expanding short axis. A detailed description of Bose-Einstein condensation using mean field theory would overcome the extend of this work but can be found in [20]. Figure 5.13 shows the radius evolution for the short (radial) and the long (longitudinal) axis and confirms what can be seen in figure 5.12.

Figure 5.14 shows linecuts of the atomic cloud of the radial axis for different EEPs after a time of flight of 10 ms. The optical density after a certain time of flight reveals the velocity distribution of the atoms in the cloud at the time the trap was still on. The big circles represent the measured data. The cyan coloured lines are Gaussian fit functions whereas the yellow lines represent bimodal fits. Here two Gaussian functions are overlaid as a bimodal fit. From bottom to top with falling EEP the data becomes more and more bimodal. The transition from a Gaussian (thermal) distribution to a bimodal distribution is, beside the inversion of the aspect ratio, a further line of evidence for the presence of a BEC [1].

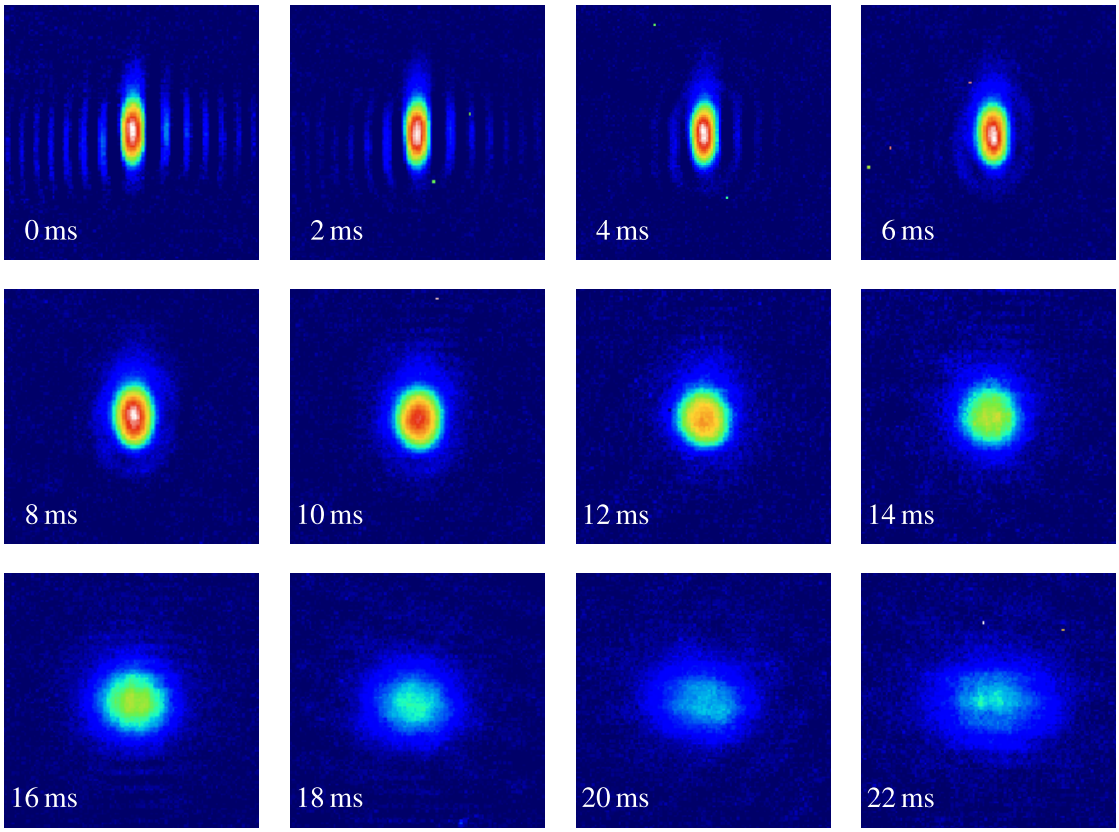

Figure 5.12: Absorption images for different time of flights. Each image is an average over 20 images. The first picture (top, left) was taken after 0 ms, the last picture (bottom, right) was taken after 22 ms time of flight. Between each picture lies 2 ms. After 16 ms a light radius inversion can be seen. In the first three images the short axis is smaller than the spatial resolution of the imaging setup which results in fringes in the first three images.

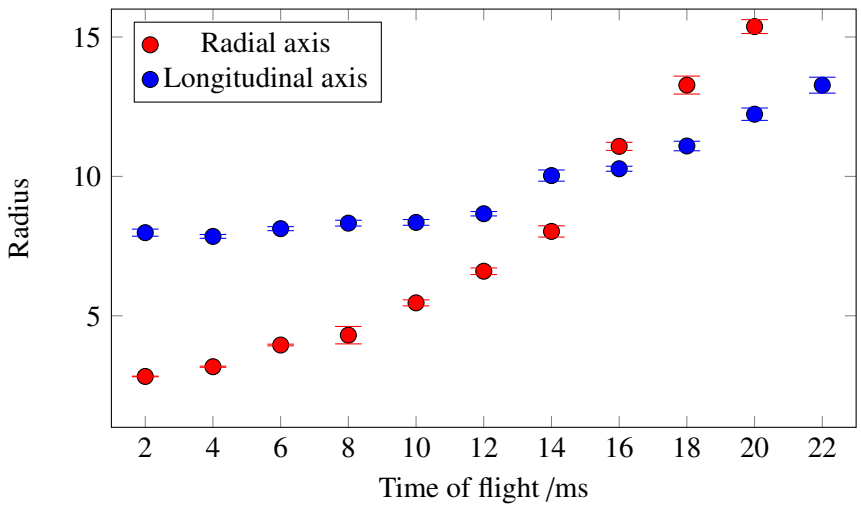

Figure 5.13: Radius development during a time of flight measurement. The initially smaller radius in radial direction expands faster than the initially larger radius in longitudinal direction caused by the larger energy gradient along the radial axis.

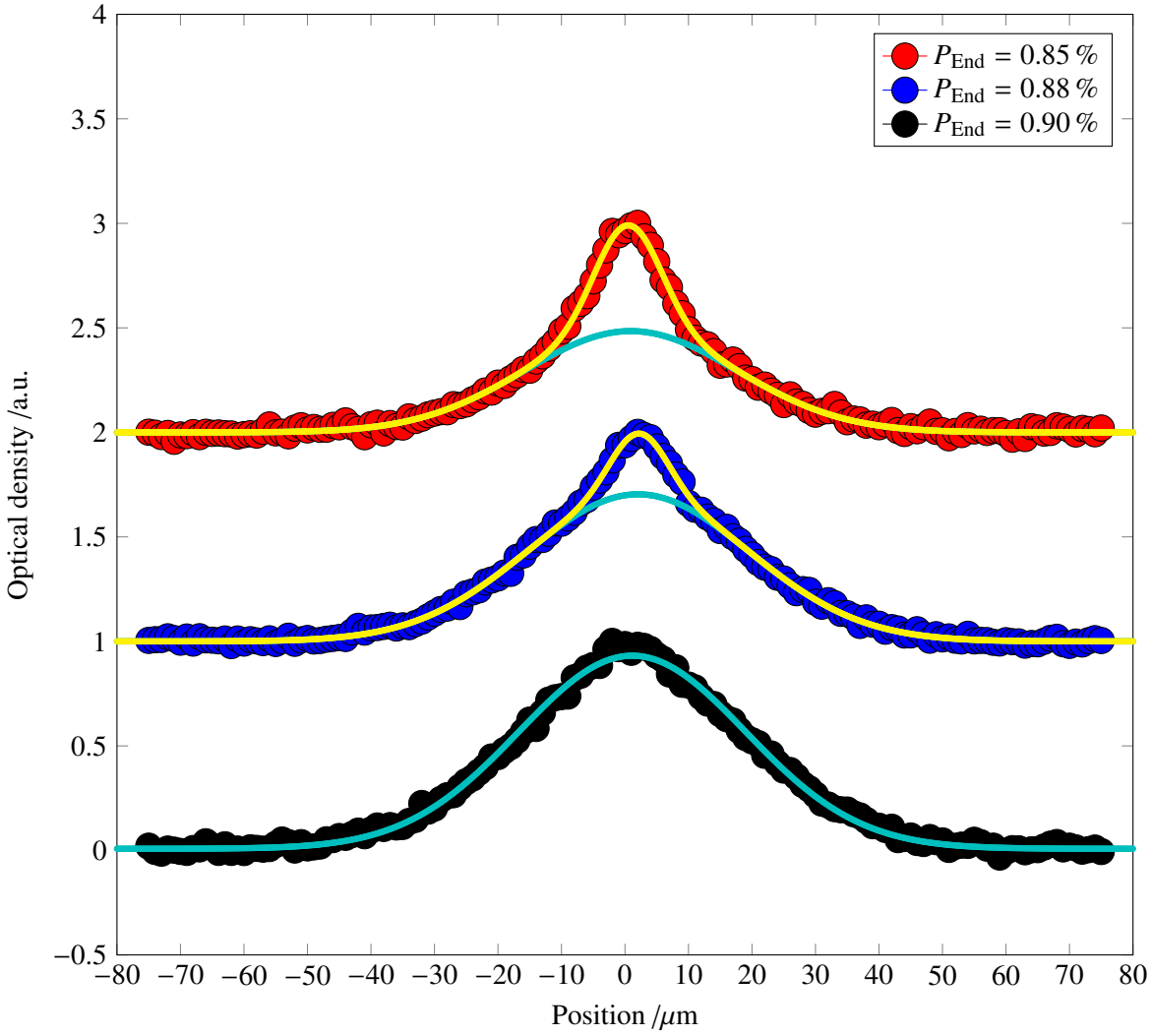

Figure 5.14: Line cuts of the atomic cloud for different EEPs. The cyan coloured fit functions represent Gaussian functions. The yellow coloured fit functions represent bimodal functions. Here two Gaussian functions are overlapped. The transition from a Gaussian distribution to a bimodal distribution is, beside the inversion of the aspect ratio, a further line of evidence for the presence of a BEC [1]. The top two data sets have an offset for clarity.

CHAPTER 6

Outlook

In the present work, based on earlier theses, an experiment able to create a Bose-Einstein condensate with erbium atoms was set up. Other groups use comparatively near resonant light [5], whereas the setup described in this thesis uses a far detuned optical dipole trap. Preliminary results regarding the characterisation of the Bose-Einstein condensate of erbium atoms were presented. The achieved peak phase space density is roughly 41. Next steps will aim to enhance the number of atoms in the Bose-Einstein condensate and to confirm the presented preliminary results.

Once the number of atoms in the Bose-Einstein condensate is enhanced a setup allowing Raman coupling between different magnetic ground states could be set up. Optical Raman transitions allow for populate different magnetic quantum states and would further give the opportunity to implement a four photon lattice like it is used by our group for experiments with ultra cold rubidum atoms [54]. Due to the non vanishing orbital angular momentum of erbium in its ground state it should be possible to drive Raman transitions with far detuned light, whereas for alkali atoms like rubidium one is restricted to near resonant light. A far detuned optical lattice should allow state dependent Raman manipulation with exceptional long coherence times. Following experiments could investigate topological edge states in amplified chirped optical lattices [55] or strong light induced gauge fields [56]. The latter could reach the fractional quantum Hall regime in two-dimensional atomic erbium microtraps.

Bibliography

[1] K. B. Davis et al., *Bose-Einstein Condensation in a Gas of Sodium Atoms*, Phys. Rev. Lett. **75**, 3969 (1995).

[2] M. H. Anderson et al., *Observation of Bose-Einstein Condensation in a Dilute Atomic Vapor*, Science **269**, 5221 198–201 (1995).

[3] S. Stellmer et al., *Bose-Einstein Condensation of Strontium*, Phys. Rev. Lett. **103**, 200401 (2009).

[4] Y. Takasu et al., *Spin-Singlet Bose-Einstein Condensation of Two-Electron Atoms*, Phys. Rev. Lett. **91**, 040404 (2003).

[5] A. Frisch, *Dipolar Quantum Gases of Erbium*, PhD Thesis: University of Innsbruck, 2014.

[6] M. Lu et al., *Strongly Dipolar Bose-Einstein Condensate of Dysprosium*, Phys. Rev. Lett. **107**, 190401 (2011).

[7] J. Klaers et al., *Bose-Einstein condensation of photons in an optical microcavity*, Nat. **468**, 7323 545–548 (2010).

[8] A. Griesmaier et al., *Bose-Einstein Condensation of Chromium*, Phys. Rev. Lett. **94**, 160401 (2005).

[9] R. Grimm, M. Weidemüller and Y. B. Ovchinnikov, *Optical Dipole Traps for Neutral Atoms*, Advances in Atomic, Molecular, and Optical Physics **42** 95–170 (2000).

[10] L. Santos et al., *Atomic quantum gases in Kagomé lattices*, Phys. Rev. Lett. **93**, 030601 (2004).

[11] M. Greiner et al., *Collapse and revival of the matter wave field of a Bose-Einstein condensate*, Nat. **419**, 6902 51–54 (2002).

[12] M. Leder, *Ultrakalte Erbiumatome in einer CO2-Laser Dipolfalle*, PhD Thesis: University of Bonn, 2016.

[13] D. Maluski, *Magneto-optical trap for erbium atoms using the narrow 583 nm transition*, Master thesis: Rheinische Friedrich-Wilhelms-Universität Bonn, 2015.

[14] J. Ulitzsch, PhD Thesis, to be published: University of Bonn.

[15] Y. Castin, "Bose-Einstein Condensates in Atomic Gases: Simple Theoretical Results", *Coherent atomic matter waves*, vol. 72, Springer, 2002 1–136.

[16] S. N. Bose, *Plancks Gesetz und Lichtquantenhypothese*, Zeitschrift für Physik **26**, 1 178–181 (1924).

[17] G. Venkataraman, *Bose and His Statistics*, Universities Press, 1992.

[18] A. Einstein, *Quantentheorie des einatomigen idealen Gases*, Sitzungsberichte der Preußischen Akademie der Wissenschaften, 1924 261–267.

[19] L. De Broglie, *The reinterpretation of wave mechanics*, Foundations of Physics **1**, 1 5–15 (1970).

[20] C. Pethick and H. Smith, *Bose-Einstein Condensation in Dilute Gases*, Cambridge University Press, 2002.

[21] J. Emsley, *The Elements*, Oxford Univiversity Press, New York, 1995.

[22] E. Worden et al., *First ionization potentials of lanthanides by laser spectroscopy*, J. Opt. Soc. Am. **68**, 1 52–61 (1978).

[23] E. A. Den Hartog, J. P. Chisholm and J. E. Lawler, *Radiative lifetimes of neutral erbium*, Journal of Physics B: Atomic, Molecular and Optical Physics **43**, 15 (2010).

[24] J. E. Lawler, J. F. Wyart and E. A. Den Hartog, *Atomic transition probabilities of Er i*, Journal of Physics B: Atomic, Molecular and Optical Physics **43**, 23 (2010).

[25] A. Kramida et al., *NIST Atomic Spectra Database (version 5.3)*, http://physics.nist.gov/asd, 2015.

[26] H. J. Metcalf and P. van der Straten, *Laser Cooling and Trapping*, Springer-Verlag, 1999.

[27] T. W. Hansch and B. Couillaud, *Laser frequency stabilization by polarization spectroscopy of a reflecting reference cavity*, Optics Communications **35**, 3 441–444 (1980).

[28] D. McCarron, S. King and S. Cornish, *Modulation transfer spectroscopy in atomic rubidium*, Measurement Science and Technology **19**, 10 (2008).

[29] D. Babik, *Frequency stabilization of a dye laser for narrow-line laser cooling of erbium atoms*, Master thesis: Rheinische Friedrich-Wilhelms-Universität Bonn, 2014.

[30] J. Schindler, *Characterization of an Erbium Atomic Beam*, Master thesis: University of Innsbruck, 2011.

[31] W. Demtröder, *Experimentalphysik 3: Atome, Moleküle und Festkörper*, Springer-Verlag, 2010.

[32] F. Arecchi and R. Bonifacio, *Theory of optical maser amplifiers*, Quantum Electronics, IEEE Journal of **1**, 4 169–178 (1965).

[33] C. Doppler, *Ueber das farbige Licht der Doppelsterne und einiger anderer Gestirne des Himmels: Versuch einer das Bradley'sche Aberrations-Theorem als integrirenden Theil in sich schliessenden allgemeineren Theorie*, Abhandlungen der k. böhm. Gesellschaft der Wissenschaften, Bd. 2, 1842 465–482.

[34] M. Rehberger, *Ultracold Erbium Atoms in Far-Detuned Optical Traps - Construction of a Zeeman-Slower*, Master thesis: Rheinische Friedrich-Wilhelms-Universität Bonn, 2013.

[35] P. Zeeman, *The Effect of Magnetisation on the Nature of Light Emitted by a Substance*, Nat. **55**, 1424 347 (1897).

[36] T. H. Loftus et al., *Narrow line cooling and momentum-space crystals*, Phys. Rev. A **70**, 063413 (2004).

[37] P. O. Schmidt, *Scattering properties of ultra-cold chromium atoms*, PhD Thesis: University of Stuttgart, 2003.

[38] H. Y. Ban et al., *Laser cooling transitions in atomic erbium*, Optics Express **13**, 8 3185–3195 (2005).

[39] S. H. Autler and C. H. Townes, *Stark Effect in Rapidly Varying Fields*, Phys. Rev. **100**, 703 (1955).

[40] A. Ashkin, *Acceleration and Trapping of Particles by Radiation Pressure*, Phys. Rev. Lett. **24**, 156 (1970).

[41] S. Chu et al.,
"Three-Dimensional Confinement and Cooling of Atoms by Resonance Radiation Pressure",
Laser Spectroscopy VII, Springer, 1985 14–17.

[42] D. Meschede, *Optik, Licht und Laser*, Springer-Verlag, 2009.

[43] T. Takekoshi, J. R. Yeh and R. J. Knize, *Quasi-electrostatic trap for neutral atoms*,
Optics Communications **114**, 5-6 421–424 (1995).

[44] C. Bolkart,
Erzeugung eines ultrakalten Gases fermionischer Kaliumatome im optischen Dipolfallenpotential,
PhD Thesis: University of Bonn, 2011.

[45] M. Lepers, J.-F. Wyart and O. Dulieu, *Anisotropic optical trapping of ultracold erbium atoms*,
Phys. Rev. A **89**, 022505 (2014).

[46] N. Masuhara et al., *Evaporative Cooling of Spin-Polarized Atomic Hydrogen*,
Phys. Rev. Lett. **61**, 935 (1988).

[47] C. S. Adams et al., *Evaporative Cooling in a Crossed Dipole Trap*,
Phys. Rev. Lett. **74**, 3577 (1995).

[48] K. M. O'hara et al., *Scaling laws for evaporative cooling in time-dependent optical traps*,
Phys. Rev. A **64**, 051403 (2001).

[49] W. Ketterle and N. J. Van Druten, *Evaporative Cooling of Trapped Atoms*,
Advances in Atomic, Molecular, and Optical Physics **37** 181–236 (1996).

[50] C.-L. Hung et al., *Accelerating evaporative cooling of atoms into Bose-Einstein condensation in optical traps*, Phys. Rev. A **78**, 011604 (2008).

[51] S. Chu et al., *Three-Dimensional Viscous Confinement and Cooling of Atoms by Resonance Radiation Pressure*, Phys. Rev. Lett. **55**, 48 (1985).

[52] J. D. Miller, R. A. Cline and D. J. Heinzen, *Far-off-resonance optical trapping of atoms*,
Phys. Rev. A **47**, R4567 (1993).

[53] D. S. Weiss et al., *Optical molasses and multilevel atoms: experiment*,
J. Opt. Soc. Am. B **6**, 11 2072–2083 (1989).

[54] G. Ritt et al., *Fourier synthesis of optical potentials for atomic quantum gases*,
Phys. Rev. A **74**, 063622 (2006).

[55] H. Brammer, *Quantensimulation von relativistischen Effekten mit ultrakalten Atomen in variablen optischen Gitterpotentialen*, PhD Thesis: University of Bonn, 2016.

[56] Y.-J. Lin et al., *Synthetic magnetic fields for ultracold neutral atoms*,
Nat. **462**, 7273 628–632 (2009).

Appendix

APPENDIX A

Appendix

A.1 ULE cavity long term drift

The atomic beam in the main chamber was illuminated with collimated 583 nm light under an angle of 90°. The lights frequency was scanned in a range of 12 MHz and the fluorescence was measured with a photomultiplier tube. A typical fluorescence measurement can be seen in figure A.1. This measurement was planned to be performed every week but due to several issues with the experiment it was performed in irregular time intervals. It turned out that the used setup was highly sensitive to the illumination angle. Even small deviations in the illumination angle resulted in different resonance frequencies due to the Doppler shift. For an angle of 89° instead of 90° the Doppler shift is already in the order of 10^9 natural line widths. Moreover it can be seen that the full width half maximum value (FWHM) of the signal is in the order of 3 MHz. The natural line width of this transition is 190 kHz.

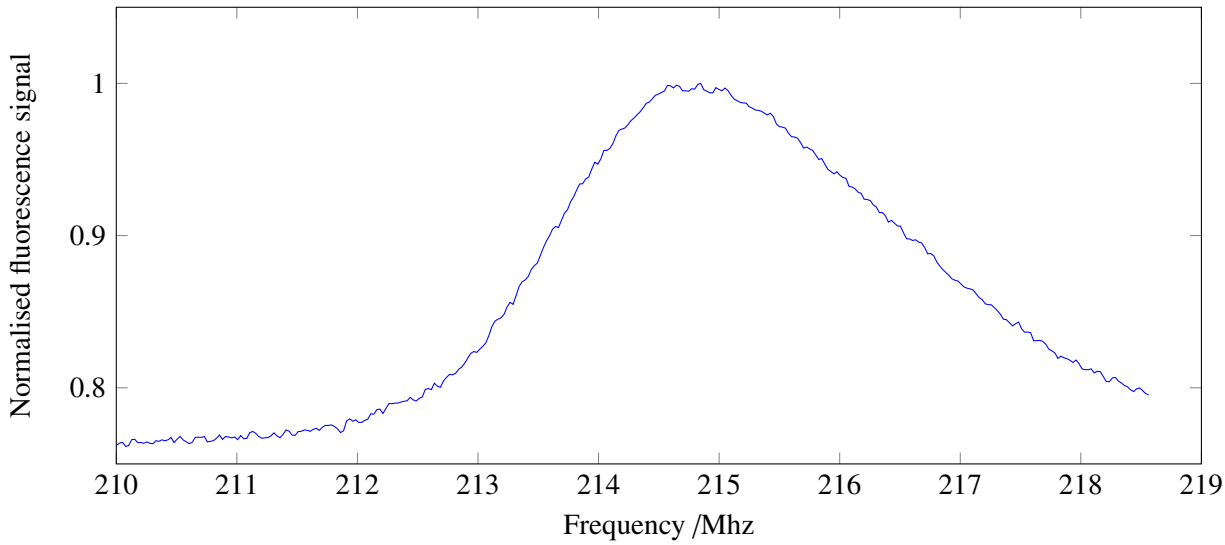

Figure A.1: Example fluorescence measurement to determine the long term drift of the ULE cavity. The peak is several linewidths broader than the transition and it's position highly sensitive to Doppler effects.

Also the main setup is more or less in its final version details change quite often and the fluorescence measurement setup which was not fully integrated into the experiment needed to be disassembled from

time to time which made it impossible to guarantee a constant illumination angle over several weeks. Another setup or method needed to be chosen.

Since an absorption imaging setup is already integrated in the setup it is more accurate to measure the resonance frequency on the atoms trapped in the MOT. The advantage is that the atoms are already cooled by the Zeeman slower and that the measurement is angle independent since the atoms are distributed isotropically inside the MOT. The only change which has to be made to the experimental setup is to switch to the 583 nm light for an absorption image. The light's frequency used for the absorption image is varied and the frequency for which the absorption is biggest determines the resonance frequency. Figure A.2 shows a resonant measurement using the absorption method with Voigt function fit. A Voigt function is the convolution of a Gaussian and a Lorentzian function. It can be seen that the peak has a FWHM of around double the natural line width of the transition. Further analysis showed that this broadening fits well to the Doppler broadening expected due to the temperature of the atoms. In order to exclude power broadening different light pulse intensities were used and it showed that there is no power broadening for the used intensity.

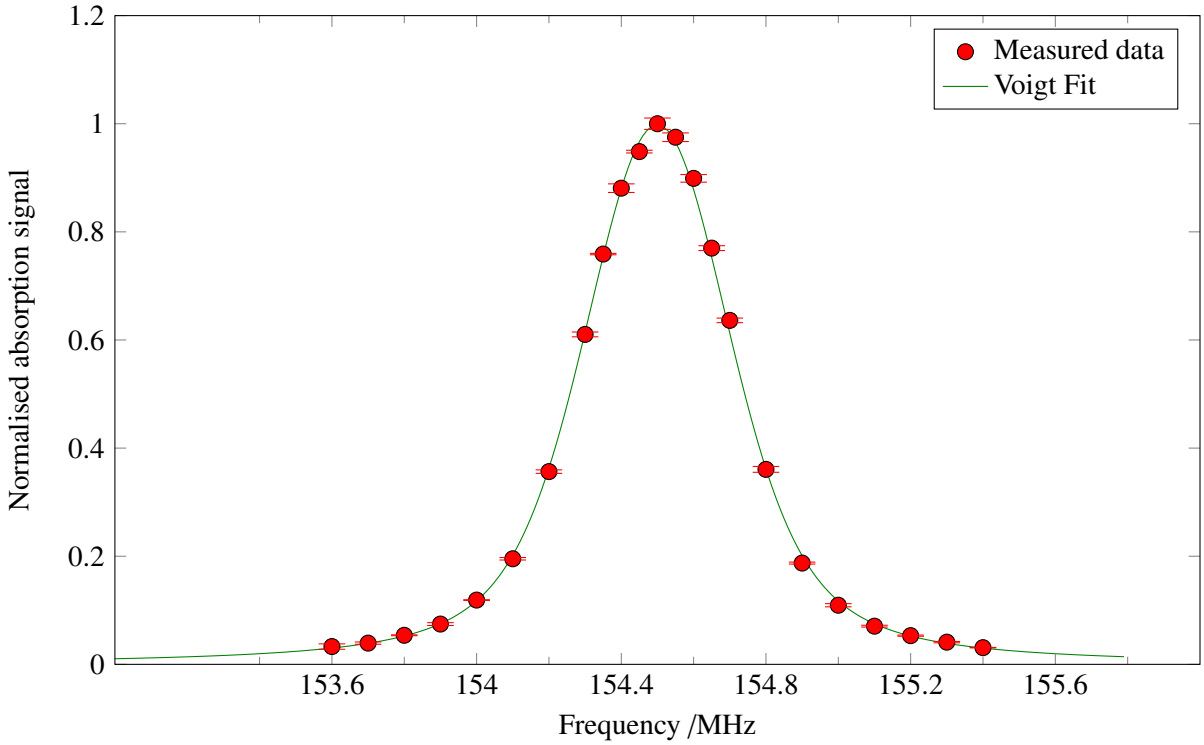

Figure A.2: Example measurement to determine the resonance frequency as function of the frequency given to the double pass AOM setup shown in figure 3.6. The resonance frequency is determined with a Voigt function fit to (154.4996 ± 0.0004) MHz.

This measurement was performed several times with approximately a week time in between. On each measurement a Voigt function was fitted to determine the resonance frequency. The resonance frequencies can be seen in figure A.3. The measurement showed that the ULE cavity has a drift of $(-9.79 \pm 0.01)\,\mathrm{kHz\,d^{-1}}$ which can be explained by the material creep. Moreover it can be seen directly that the errors on the measurement points are really small which give rise to doubts if the error calculations are correct. The errors have their origin in the measured atom number which is determined by the optical

density of the absorption image. The Voigt fit onto the atom numbers for different frequencies considers these errors. One external effect which is not included up to now is the temperature of the ULE cavity. Even though the ULE cavity is temperature stabilised the temperature changes during the day. The laboratory gets slightly warmer when the experiment is running. This temperature shift results in a drift of the resonant frequency of the cavity by $\nu_{\text{Drift}} = (1.23 \pm 0.01)\,\text{kHz}\,\text{d}^{-1}$ and was measured in [29]. This drift needs to be included in the future. Moreover the cooling system failed for a day and it takes up to a few days for the ULE cavity to have a stable temperature and with that a stable cavity length.

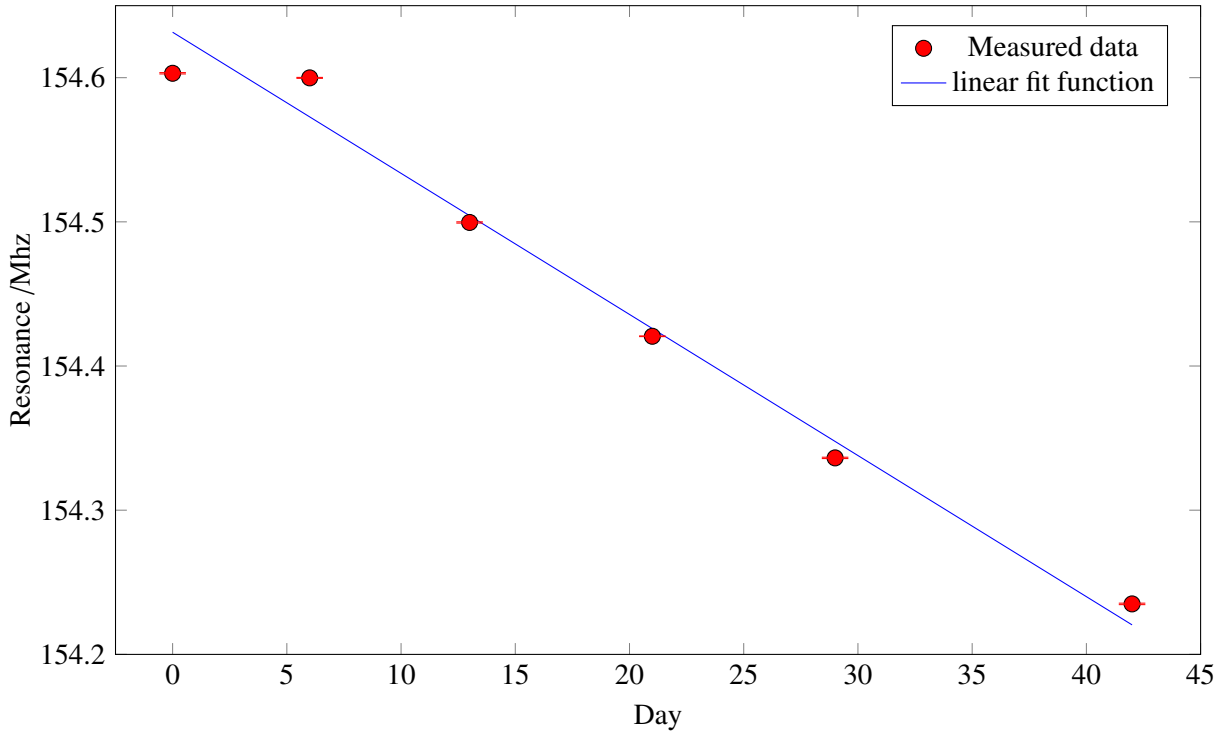

Figure A.3: Change in resonance frequency as function of past days measured by absorption signals. The frequency is given onto a double pass AOM setup to shift the 583 nm light's frequency which is stabilised by the ULE cavity in order to be resonant with the 583 nm transition. The slope of the linear fit represents the drift per day of the ULE cavity due to the material creep. The drift of the ULE cavity is $(-9.79 \pm 0.01)\,\text{kHz}\,\text{d}^{-1}$.

Danksagung

Das Verfassen einer Abschlussarbeit ist immer mit der Hilfe anderer Personen verbunden. Aus diesem Grund würde ich gerne einigen Menschen danken.

An erster Stelle möchte ich Prof. Dr. Martin Weitz dafür Danken, mir die Möglichkeit gegeben zu haben meine Masterarbeit in seiner Arbeitsgruppe anzufertigen. Der Austausch zwischen Professor und Studenten ist in dieser Arbeitsgruppe sehr groß. Fast täglich erscheint Martin im Labor und erkundigt sich nach dem aktuellen Stand der Dinge. Dadurch ist er bei der Lösung vieler Probleme unmittelbar beteiligt. Regelmäßige Gruppentreffen sichern zusätzlich einen regen Austausch innerhalb der Gruppe und den verschiedenen Experimenten. Ich freue mich sehr meine akademische Laufbahn in dieser Gruppe mit einer Doktorandenstelle weiter fortzuführen.

Desweiteren möchte ich Priv.-Doz. Dr. Elisabeth Soergel danken. Ohne zu zögern erklärte sie sich bereit, die Zweitkorrektur meiner Masterarbeit zu übernehmen. Neben dem Bereiterklären die Zweitkorrektur zu übernehmen, gab Elisabeth mir eine Menge Rat in Bezug auf meine weitere akademische Laufbahn.

Weiterhin möchte ich den Personen danken, mit denen ich sehr viel Zeit im Labor verbracht habe. Hierbei an erster Stelle Jens Ulitsch. Es gab eine Menge Tage, an denen ich mit Jens mehr Zeit im Labor verbrachte als mit meiner Frau zu Hause. Von Jens konnte ich eine Menge bezüglich des experimentellen Aufbaus, experimenteller Methoden und der zugrunde liegenden Physik lernen. Ich möchte auch Daniel Babik danken. Es macht immer Spaß mit ihm zusammen im Labor zu arbeiten und das Experiment vorran zu bringen. Auch von ihm lernte ich eine Menge und ich freue mich weiterhin mit ihm zusammen zu arbeiten. Desweiteren möchte ich Dr. Martin Leder danken. Nachdem Martin seine Doktorarbeit einreichte, half er uns auf den letzten Schritten zum Bose-Einstein Kondensat. Seine Erfahrung mit Ultrakalten-Atomen war besonders hilfreich. Eine weitere wichtige Person ist Dr. Henning Brammer. Auch wenn ich relativ wenig Zeit mit ihm im Labor verbrachte, so war es immer informativ und lehrreich.

Eine Person, der vermutlich jeder der im Institut für angewandte Physik einen Abschluss beendet danken muss, ist Dr. Frank Vewinger. Frank ist zwar so gut wie nie zu finden da er immer beschäftigt ist, findet man ihn aber, kann man sich sicher sein, dass er einem weiterhelfen kann.

Ich möchte der ganzen Arbeitsgruppe danken. Der außergewöhnliche Teamgeist in dieser Gruppe ist meiner Ansicht nach einer der Schlüsselaspekte für den Erfolg dieser Gruppe. Ich freue mich auch weiterhin ein Mitglied dieses Teams zu sein.

Zu guter Letzt möchte ich meiner Familie danken. Die ganzen Jahre des Physikstudium waren nicht nur spaßig und interessant, sondern sehr oft auch einfach nur anstrengend und hier und da auch frustrierend. Meine Familie stand immer hinter mir und hat mich in jeder Entscheidung vollstens unterstützt. Manche Dinge sind ein wenig leichter wenn man weiß, dass man nicht alleine ist. Selbiges gilt für meine Frau. Ohne meine Frau wäre vieles noch schwieriger gewesen. Sie unterstützt mich in jeder Hinsicht und sagt mir auch von Zeit zu Zeit, dass es Zeit für eine Pause ist. Sie hat einen Instinkt dafür, wann dieser Zeitpunkt gekommen ist. Ich hoffe, ich kann Sie in ihren Abschlussprüfungen genauso unterstützen, wie sie mich die letzten Wochen unterstützt hat.

Danke!